ACIBADEM MEHMET ALI AYDINLAR UNIVERSITY
INSTITUTE OF HEALTH SCIENCES

INVESTIGATION OF SIGNALING PATHWAYS ACTIVATED BY THE ORPHAN G PROTEIN-COUPLED RECEPTOR GPR37

GÖKNUR EROL

M.Sc. THESIS

DEPARTMENT OF BIOPHYSICS

SUPERVISOR
Prof. Dr. Beki KAN

ISTANBUL-2025

ACIBADEM MEHMET ALI AYDINLAR UNIVERSITY
INSTITUTE OF HEALTH SCIENCES

INVESTIGATION OF SIGNALING PATHWAYS ACTIVATED BY THE ORPHAN G PROTEIN-COUPLED RECEPTOR GPR37

GÖKNUR EROL

M.Sc. THESIS

DEPARTMENT OF BIOPHYSICS

SUPERVISOR
Prof. Dr. Beki Kan

ISTANBUL-2025

DECLARATION

I declare that this thesis work is my own work, I had no unethical behavior at any stages from the planning to the writing of the thesis, I obtained all the information in this thesis in accordance with academic and ethical rules, I cited all the information and comments that were not obtained with this thesis work, and I provided resources in the list of references. I also declare that there was no violation of any patents and copyrights during the study and writing of this thesis.

03/02/2025

Göknur Erol

PREFACE AND ACKNOWLEDGEMENT

I would like to express my deepest gratitude to my supervisor, Prof. Dr. Beki Kan, for her insightful guidance, patience, and invaluable mentorship in helping me navigate the challenges of this research. I am also grateful to Prof. Dr. Devrim Öz Arslan for her suggestions and help throughout this study. I am also thankful to Assoc. Prof. Zeynep Aslıhan Durer for her contributions. I could not have undertaken this journey without my wonderful lab colleagues Kaan Biçici, Ghazal Footohi, Şeyma Elbeyoğlu, Evrim Zeren, Ceren Çelik who made this journey so much better with their kindness, humor, and support. To Berra Ateşok, I am endlessly grateful for your unwavering support and constant willingness to help, especially during moments when things did not go as planned. To Berkcan Koç, thank you for being there to support each other through the tough times.

I must also express my deepest appreciation to my family, especially my parents, Ekrem Erol and Havva Erol, for believing in me every step of the way. My appreciation also goes to my dearest friends, Berfu Karakuş and Ezgi Atalay for providing the perfect balance to my life with laughter and meaningful conversations.

I would also like to thank Acıbadem Mehmet Ali Aydınlar University for providing laboratory facilities and to Scientific and Technological Research Council of Turkey (TUBITAK) for their financial support.

I would like to express my gratitude to Dr. Erdinç Sezgin and his team at SciLifeLab in Sweden for the valuable research experience during my stay as an ERASMUS+ trainee. I would also like to extend my sincere thanks to my supervisor Dr. Pablo Carravilla for his insightful guidance and support.

This study was supported by TUBITAK 1002-B project (124Z387) and Acıbadem University (ABAPKO TYL-2023-2152 and THD-2023-2189). I was supported by TUBITAK BIDEB 2210-A Scholarship Program from 2022 to 2024.

TABLE OF CONTENTS

ABBREVIATIONS AND SYMBOLS

2D	Two-dimensional
3D	Three-dimensional
4-PBA	4-phenylbutyrate
AD	Alzheimer's disease
APS	Ammonium persulfate
ATP	Adenosine triphosphate
BB1, BB2	Bombesin receptors
BSA	Bovine serum albumin
cAMP	Second messenger cyclic AMP
CO_2	Carbon dioxide
DAG	Diacylglycerol
dH_2O	Double distilled water
DMSO	Dimethyl sulfoxide
dPBS	Dulbecco's phosphate-buffered saline
DTT	Dithiothreitol
ECL	Extracellular loop
EDTA	Ethylenediaminetetraacetic acid
ER	Endoplasmic reticulum
ERK	Extracellular signal-regulated kinase
FBS	Fetal bovine serum
FCS	Fluorescence correlation spectroscopy
FITC	Fluorescein isothiocyanate
GDP	Guanosine diphosphate
GPCR	G protein-coupled receptor
GPMVs	Giant plasma membrane vesicles
GPR37	G-protein-coupled receptor 37
GPR37L1	G-protein-coupled receptor 37-like 1
GRK	G-protein-coupled receptor kinase
GTP	Guanosine triphosphate
HA	Head activator

HCl	Hydrochloric acid
H_2O	Water
HRP	Horseradish peroxidase
ICL	Intracellular loop
IgG	Immunoglobulin G
IP3	Inositol 1,4,5-trisphosphate
KCl	Potassium chloride
Kda	Kilodalton
KH_2PO_4	Potassium phosphate monobasic
LB	Liquid broth
LPS	Lipopolysaccharide
µg	Microgram
µl	Microliter
µm	Micrometer
µM	Micromolar
MAPK	Mitogen-activated protein kinase
MEC	Mammary epithelial cell
mg	Milligram
min	Minutes
ml	Milliliter
mM	Millimolar
mTOR	Mammalian target of rapamycin
MTT	3-(4,5-dimethylthiazol-2-yl)-2,5-diphenyl tetrazolium bromide
NaCl	Sodium chloride
NC	Nitrocellulose
NFAT	Nuclear factor of activated T-cell reporter
NaF	Sodium fluoride
ng	Nanogram
$Na_2HPO_4.12H_2O$	Sodium phosphate dibasic dodecahydrate
nm	Nanometer
nM	Nanomolar

NaOH	Sodium hydroxide
Na_3VO_4	Sodium orthovanadate
NPD1	Neuroprotectin D1
PBS	Phosphate-buffered saline
PBST	Phosphate-buffered saline Tween
PI	Protease inhibitor
PI3	Phosphoinositide 3-kinase
PIP2	Phosphatidylinositol 4,5-bisphosphate
PKA	Protein kinase A
PKC	Protein kinase C
PLCβ	Phospholipase C β
PMA	Phorbol-12-myristate-13-acetate
PMSF	Phenylmethylsulfonyl fluoride
PSAP	Prosaposin
PVDF	Polyvinylide Fluoride
RhoGEFs	Rho guanine nucleotide exchange factors
RIPA	Radioimmunoprecipitation assay
rPSAP	Recombinant PSAP
RTKs	Receptor tyrosine kinases
SD	Standard deviation
SDS	Sodium dodecyl sulfate
SDS-PAGE	Sodium dodecyl sulfate polyacrylamide gel electrophoresis
TEMED	Tetramethylethylenediamine
TX14A	Prosaptide
V	Volts

LIST OF FIGURES

LIST OF TABLES

ABSTRACT

Investigation of Signaling Pathways Activated by the Orphan G Protein-Coupled Receptor GPR37

G Protein-Coupled Receptor 37 (GPR37) has attracted attention due to its role in neuroprotection and its potential as a therapeutic target in neurodegenerative diseases. Prosaposin and its synthetic derivative prosaptide TX14(A) are a potential ligand of GPR37, and its effects on cellular signaling pathways of GPR37 remain under exploration. This study explores the downstream impacts of prosaptide-activated GPR37 on the PI3K-AKT-mTOR signaling pathway. GPR37 activation led to increased phosphorylation of PI3K p85 and mTOR, but a decrease in p70S6K and AKT phosphorylation in GPR37-transfected cells, indicating complex regulation of the pathway. Furthermore, upon prosaptide treatment, GPR37 displayed dynamic changes in its localization, shifting from the plasma membrane to intracellular regions. The diffusion properties of GPR37 were also investigated using fluorescence correlation spectroscopy (FCS) and giant plasma membrane vesicles (GPMVs). The diffusion coefficient of GPR37 in cells was higher than anticipated for membrane-bound receptors, potentially due to their retention in intracellular compartments. In GPMVs, GPR37 demonstrated lower diffusion coefficients, reflecting the behavior of membrane proteins in a simplified lipid bilayer environment, free from intracellular complexities.

These observations suggest that GPR37 exhibits complex trafficking behavior and diffusion dynamics. While prosaptide activation provides insight into the potential modulation of key cellular pathways, further research is needed to fully uncover the intricate mechanisms underlying GPR37's biological roles.

Keywords: G Protein Coupled Receptor, GPR37, Prosaptide, PI3K-AKT-mTOR, Signaling

ÖZET

Yetim G Protein-Kenetli Reseptör Ailesine ait GPR37'nin Aktive Ettiği Sinyal Yolaklarının İncelenmesi

G Protein-Kenetli Reseptör 37 (GPR37), nörokorumadaki rolünden ve nörodejeneratif hastalıkların tedavisinde potansiyel terapötik hedef olmasından dolayı dikkat çekmektedir. Prosaposin ve onun sentetik türevi olan prosaptit TX14(A), GPR37'nin potansiyel bir ligandı olarak öne çıkmakta ve bunların GPR37'nin hücresel sinyal yolakları üzerindeki etkileri hâlâ araştırılmaktadır. Bu çalışma, prosaptit ile aktive edilen GPR37'nin PI3K-AKT-mTOR sinyal yolağındaki etkilerini incelemektedir. GPR37 aktivasyonu, PI3K p85 ve mTOR fosforilasyonunda artışa, ancak p70S6K ve AKT fosforilasyonunda azalmaya yol açarak, bu yolağın karmaşık bir şekilde düzenlendiğini göstermektedir. Ayrıca, prosaptit ile muamele edildikten sonra GPR37, plazma membranından hücre içi bölgelere geçerek lokalizasyonunda dinamik değişiklikler göstermiştir.

GPR37'nin difüzyon özellikleri ayrıca floresan korelasyon spektroskopisi (FCS) ve dev plazma membran vezikülleri (GPMV'ler) kullanılarak araştırıldı. GPR37'nin hücrelerdeki difüzyon katsayısı, muhtemelen hücre içi bölümlerde tutulması nedeniyle, membrana bağlı reseptörler için beklenenden daha yüksek çıkmıştır. GPMV'lerde GPR37, hücre içi karmaşıklıklardan bağımsız, daha sade bir lipid çift katmanlı ortamda, membran proteinlerinin tipik davranışına uygun olarak daha düşük difüzyon katsayıları sergilemiştir.

Bu gözlemler, GPR37'nin karmaşık trafik davranışı ve difüzyon dinamikleri sergilediğini göstermektedir. Prosaptit aktivasyonu, önemli hücresel yolaklarının potansiyel modülasyonuna dair fikir verirken, GPR37'nin biyolojik rollerinin altında yatan karmaşık mekanizmaları tam olarak ortaya çıkarmak için daha fazla araştırmaya ihtiyaç vardır.

Anahtar Sözcükler: G Protein Kenetli Reseptör, GPR37, Prosaptide, PI3K-AKT-mTOR, Sinyalleşme

1 INTRODUCTION AND AIM

G protein-coupled receptors (GPCRs) represent the largest group of membrane proteins, playing a crucial role in regulating cellular signal transduction mechanisms activated by hormones, neurotransmitters, ions, lipids, as well as photons and odorants [1]. Therefore, they represent the largest group among drug targets. Although ligands and effectors are known for many of these receptors, some GPCRs are referred to as "orphans" because they have not yet been paired with their endogenous ligands [2].

Among these, G-protein-coupled receptor 37 (GPR37), also known as parkin-associated endothelin B receptor-like receptor (PaelR), is of interest because it has been associated with several diseases such as autosomal recessive juvenile Parkinsonism, autism, epilepsy, and bipolar disorders [3, 4]. However, the signaling pathways and physiological functions of GPR37 have not been fully elucidated.

Prosaptide (TX14(A)), a synthetic peptide derived from prosaposin, is known to be one of the proposed ligands of GPR37 [5]. This peptide has been shown to exert neuroprotective effects by activating pathways that promote cell survival and repair [6, 7]. One of the triggered downstream signaling pathways, PI3K-AKT, is a critical regulator of cellular processes, including metabolism, growth, and survival [8].

When misfolded or overexpressed, GPR37 tends to form intracellular aggregates, leading to its inefficient trafficking to the plasma membrane [9, 10]. This misfolding impairs its functional expression and cellular localization. Giant plasma membrane vesicles (GPMVs) could provide a stable system for studying membrane-bound proteins like GPCRs, offering an environment that isolates the plasma membrane from the complexities of the intracellular environment [11].

In this study, we aimed to explore the function of the orphan GPR37 in cellular signaling processes. To this end, HEK293T cells overexpressing GFP-tagged GPR37 and YFP-tagged GPR37 will be treated with prosaptide, and the activation of the phosphoinositide 3-kinase/Akt (PI3K/Akt) signaling pathway by the GPR37-

prosaptide interaction will be investigated. Finally, GPMVs derived from GPR37-transfected HEK293T cells will be used to study the diffusion properties and membrane dynamics of the receptor, providing further insights into its behavior in an environment isolated from the intracellular milieu, using fluorescence correlation spectroscopy (FCS).

2 BACKGROUND

2.1 G-Protein Coupled Receptor (GPCRs)

Intercellular communication relies on various signaling molecules, such as neurotransmitters, hormones, and growth factors. These chemical messengers interact with specific receptors embedded in the plasma membranes of target cells, initiating precise cellular responses. G protein-coupled receptors (GPCRs) are the largest and most diverse membrane receptor family, consisting of more than 800 receptors, corresponding to %2-3 of the human genome [12]. GPCRs initiate cellular responses by activating their associated G proteins located on the intracellular face of the cell membrane. These G proteins mediate signaling via various intracellular effectors, leading to a cascade of molecular events [13]. These events regulate numerous physiological processes including sensory perception, neuronal signal transmission, hormonal regulation, cell growth, and cellular differentiation [14].

While GPCRs display remarkable diversity in their functions and regulatory mechanisms, they all share a characteristic tertiary structure composed of seven transmembrane-spanning (7TM) α-helices, connected by three intracellular (named ICL1-3) and three extracellular loops (ECL1-3) [1]. These receptors, which traverse the plasma membrane, have their amino (N) terminus exposed to the extracellular side and their carboxyl (C) terminus facing the intracellular side [15, 16, 17].

GPCRs can respond to a wide variety of stimuli including endogenous (biogenic amines, ions, lipids, peptides, and glycoproteins) and exogenous (photons, therapeutic drugs, pheromones, and odorants) ligands [18, 19]. Impaired concentrations of GPCR ligands, abnormal receptor expression, and mutations in GPCRs can disrupt cellular processes and contribute to many pathophysiological conditions, including central nervous system disorders, neurodegenerative diseases, cardiovascular and respiratory diseases, gastrointestinal and metabolic disorders, immune diseases, cancer, and eye diseases [20, 21]. Therefore, GPCRs represent one of the most important therapeutic targets in modern medicine, as these receptors target approximately 30-40% of

currently prescribed drugs [22]. The importance of GPCR studies in signal transduction has been widely recognized and valued in medical and life sciences research. This significance was highlighted in 2012 when Robert J. Lefkowitz and Brian Kobilka were awarded the Nobel Prize in Chemistry for their groundbreaking GPCR research [23, 24]. Lefkowitz, a pioneer in the field for over four decades, established many fundamental concepts in GPCR biology. A breakthrough came in 2007 when Kobilka determined the crystal structure of the β2-adrenergic receptor, an achievement that paved the way for elucidating the structures of more than 50 GPCRs.

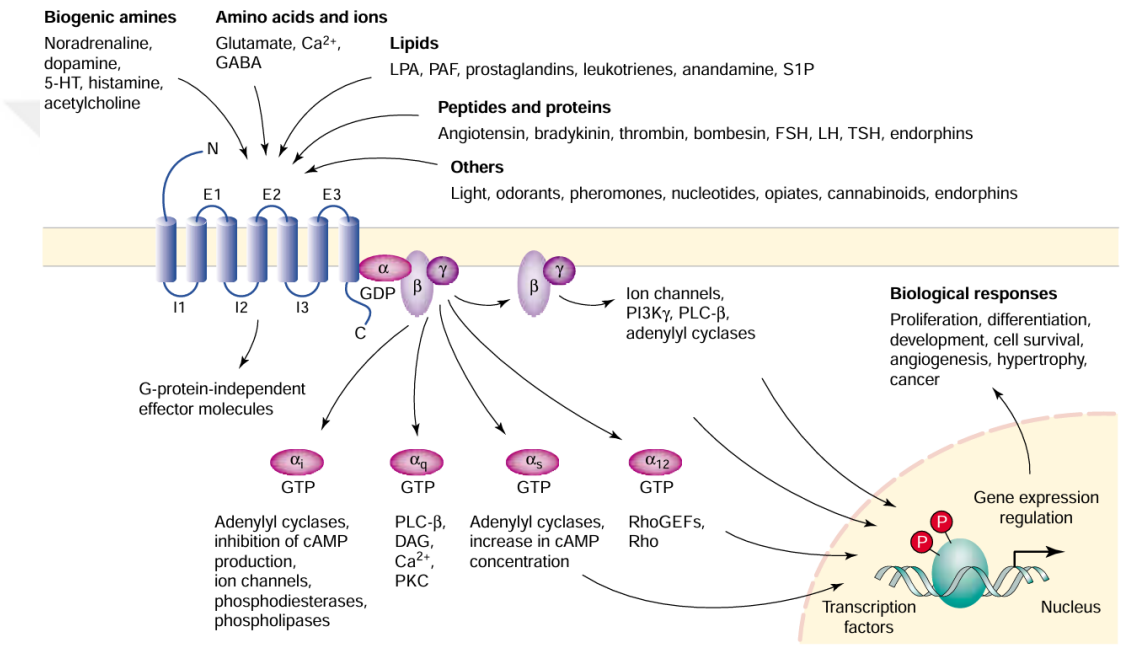

Figure 1. Diversity of ligands for GPCRs [18].
A wide variety of ligands bind to GPCRs and activate various signaling pathways to regulate biological responses.

2.2 GPCR Classification

GPCRs are classified based on their sequence homology and phylogenetic origin (structural and functional characteristics). Although GPCRs do not share overall sequence homology, there is significant sequence homology within some GPCR subfamilies [25, 26]. The Nomenclature Committee of the International Union of Basic and Clinical Pharmacology (NC-IUPHAR) divides GPCRs into six classes based on sequence homology: Class A(rhodopsin-like), Class B (secretin receptor family), Class

C (metabotropic glutamate), Class D (fungal mating pheromone receptors), Class E (cyclic AMP receptors) and Class F (frizzled/smoothened) [27]. Alternatively, GRAFS classification system divides GPCRs into five classes based on phylogenetic studies: Glutamate (G), Rhodopsin (R), Adhesion (A), Frizzled/Taste2 (F), and Secretin (S) [28].

2.3 GPCR Signaling

While GPCRs are primarily known for their ability to bind ligands and activate heterotrimeric G proteins (Gαβγ), they also engage in G-protein-independent signaling pathways by G-protein-coupled receptor kinase (GRK)-mediated phosphorylation and arrestin coupling.

2.3.1 G-Protein dependent signaling

Heterotrimeric G proteins act as a transducer of signals initiated by ligand-receptor coupling, triggering conformational changes in the receptor that promote the activation of associated G protein [29]. In the heterotrimeric inactive state, the G protein is composed of three subunits— Gα and Gβ, Gγ, with the α subunit bound to guanosine diphosphate (GDP). The receptor and G protein trimer remain separate on the membrane until ligand binding shifts the conformation of the receptor, increasing its affinity for the αβγ trimer. Upon receptor activation, the α subunit of G protein releases GDP and instead binds to guanosine triphosphate (GTP). This GDP/GTP exchange leads to the dissociation of Gα from both the Gβγ dimer and the GPCR itself [30].

GPCRs activate numerous intracellular signaling pathways through GTP-bound α subunits and released Gβγ dimers. G-proteins can be grouped into four major families according to the Gα-subunit**:** $G\alpha_s$, $G\alpha_i$, $G\alpha_q$, and $G\alpha_{12/13}$ [31]. Each family mediates the regulation of diverse physiological processes in response to extracellular signals.

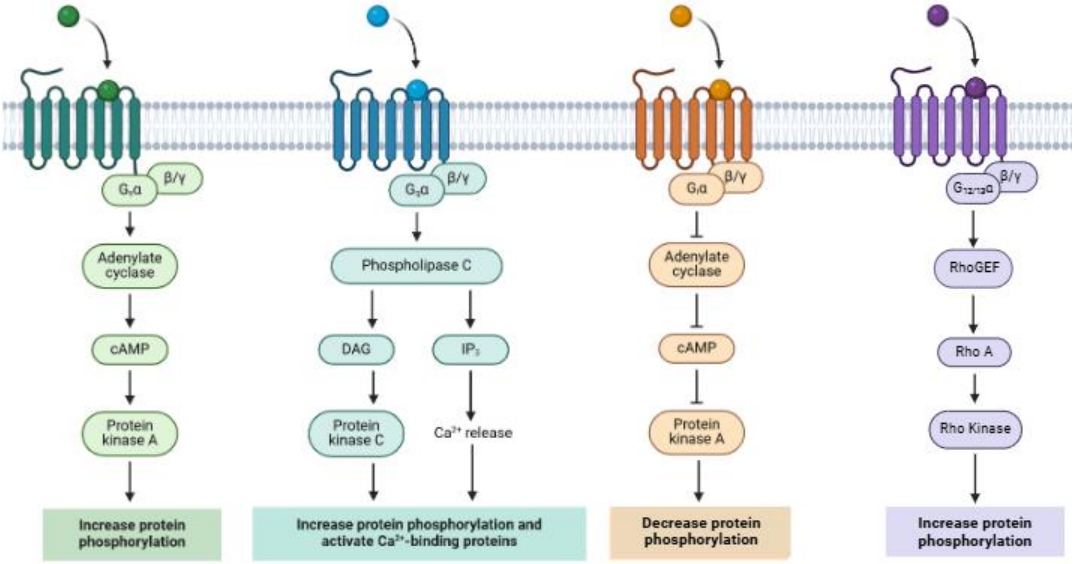

Figure 2. G protein-dependent signaling pathways of $G\alpha_q$, $G\alpha_s$, $G\alpha_i$, and $G\alpha_{12/13}$ protein families [32].

The $G\alpha_s$ family of G proteins directly stimulates membrane-associated adenylate cyclase, leading to increased second messenger cyclic AMP (cAMP) levels by breaking down adenosine triphosphate (ATP) and subsequent activation of protein kinase A (PKA). Once activated, PKA can phosphorylate target proteins resulting in a variety of downstream effects. In contrast, $G\alpha_i$ inhibits adenylyl cyclase and therefore decreases cAMP production from ATP.

$G\alpha_q$ proteins activate phospholipase C β (PLCβ), which catalyzes the production of inositol 1,4,5-trisphosphate (IP_3) and diacylglycerol (DAG) from the membrane phospholipid phosphatidylinositol 4,5-bisphosphate (PIP_2). IP_3 binds to IP_3 receptors in the endoplasmic reticulum and results in Ca^{+2} release into the cytoplasm. DAG activates the protein kinase C (PKC) [33, 34].

Finally, the $G_{12/13}$ family activates Rho guanine nucleotide exchange factors (RhoGEFs), which in turn activate the Rho family of small GTPases, including RhoA. Once activated, RhoA regulates several downstream effectors such as Rho kinases [35, 36].

β/γ complexes are now recognized for their role in mediating many functions including recruiting GRKs to the membrane, regulating G-protein-coupled inwardly rectifying potassium channels and adenylyl cyclases [37, 38].

2.3.2 G-Protein independent signaling

GPCRs have been studied primarily for their canonical signaling through G protein-dependent mechanisms. However, recent studies have shown that GPCRs can also signal through G protein-independent pathways, engaging non-G protein signaling effectors that do not rely on traditional G protein interactions. Apart from heterotrimeric G proteins, two protein families interact with activated GPCRs: G protein-coupled receptor kinases (GRKs) and β-arrestins [39].

GRKs and β-arrestins have been involved in GPCR desensitization and internalization/recycling [40]. Upon ligand binding and receptor activation, GRKs phosphorylate specific residues on the intracellular domains of GPCRs which promotes the binding of β-arrestin to the activated receptor. This GPCR-β-arrestin interaction blocks the G protein binding site which prevents prolonged receptor activation and thereby contributes to GPCR desensitization [41, 42]. Additionally, the receptor-arrestin complexes are targeted for clathrin-mediated endocytosis [43]. Depending on the interaction, the receptors can either be recycled to the plasma membrane, internalized into endosomes, or targeted for degradation [44]. This dynamic regulatory mechanism is crucial for maintaining cellular homeostasis as any dysfunction could result in variety of disorders such as heart failure and Parkinson's disease [45, 46].

In addition to GPCR regulation, both GRKs and β-arrestins have been demonstrated to contribute to signal transduction, independently of G proteins. They act as scaffold proteins to activate mitogen-activated protein kinases (MAPKs)/ERK signaling cascade and Src family tyrosine kinases [47, 39].

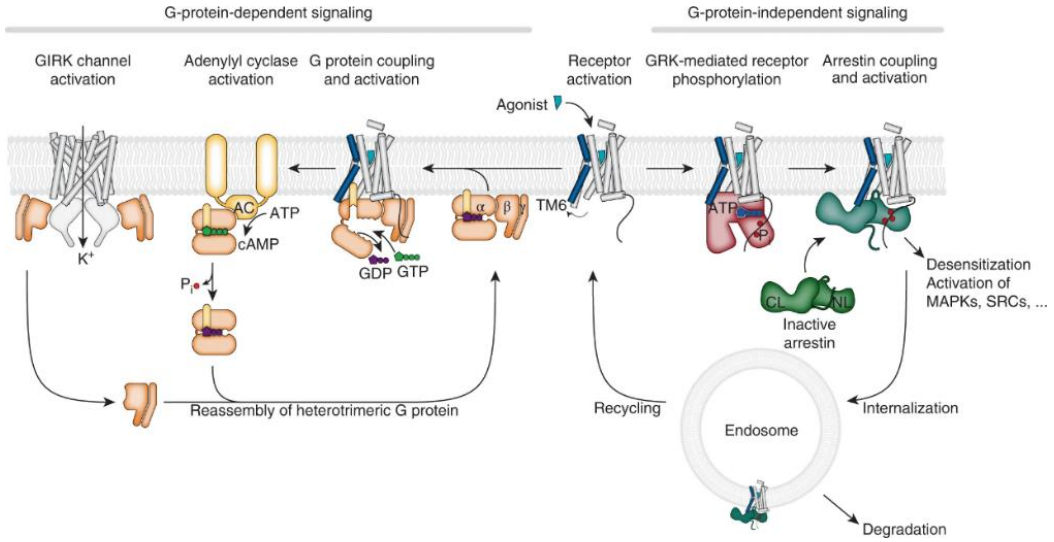

Figure 3. G protein-dependent and independent signaling pathways [48].

2.4 Orphan GPCRs

GPCRs are the most successful drug targets because they bind and respond to agonists, antagonists, and allosteric modulators and induce functional cellular responses. Nevertheless, a significant number of GPCRs have not been matched with their endogenous ligands. In 2004, the human genome sequencing identified over 800 GPCRs of which about 140 receptors have not yet been paired with their endogenous ligands [49, 50, 51]. Thus, the functions of these receptors remain unknown. These are called “orphan” GPCRs. Because only approximately 10% of GPCRs are suitable to be therapeutic targets, the de-orphanisation of orphan GPCRs that is, pairing with their endogenous ligand(s), emerges as a promising approach for the treatment of many diseases [52, 53].

International Union of Basic and Clinical Pharmacology (IUPHAR) considers a receptor as deorphanized based on two criteria: Firstly, two or more independent research groups must publish peer-reviewed papers showing the activity of ligand-receptor interaction, at potencies consistent with a physiological function. Evidence of ligand-receptor binding and functional activation should be provided with a diverse array of assays such as radio-ligand binding, calcium flux, and modulation of cAMP levels [54, 55]. Reproducibility of the pairing is crucial to avoid false positive results.

If two independent laboratories report ligand-receptor interaction but the third one fails to confirm that, IUPHAR requires further investigation to eliminate controversy [56].

Secondly, the tissues must have sufficient levels of the proposed endogenous ligand. There should be mechanisms for the ligand to reach physiologically significant concentrations for the receptor. Indirect techniques such as immunocytochemistry can validate GPCR-ligand pairings for neuropeptides. The concentration of small molecule ligands can be determined using radioimmunoassay or mass spectrometry associated with gas chromatography or high-performance liquid chromatography [56, 2].

The proposed pharmacological link between an endogenous ligand and its cognate receptor can be tested where the orphan GPCR expression has been ablated or increased using genetically engineered mice [56]. The use of genetic manipulation approaches should alter receptor characteristics, supporting the ligand-receptor pairing. Receptor overexpression and deletion can also provide evidence for a pathophysiological role. For example, GPR3 is extensively expressed in the central nervous system and is involved in Alzheimer's disease (AD) [57]. GPR3 is thought to play a role in the regulation of amyloid precursor protein and the production of amyloid-beta peptides which is one of the hallmarks of AD pathology. In AD mouse models, GPR3 deletion has been linked to reduced amyloid-beta production, while overexpression of the receptor increases amyloid-beta production [58]. These results indicate that GPR3 might be a valuable therapeutic target for Alzheimer's disease.

2.5 G-Protein Coupled Receptor 37

Orphan G-protein-coupled receptor 37 (GPR37), also known as parkin-associated endothelin B receptor-like receptor (PaelR), is predominantly expressed in the mammalian central nervous system particularly in the corpus callosum, striatum, and substantia nigra, while having minimal peripheral expression [3]. Within the brain, the receptor is specifically found in late-stage (pre-myelinating and myelinating) oligodendrocytes, mature astrocytes, and dopaminergic neurons of the substantia nigra

[59, 9]. Low levels of GPR37 are detected in the human kidney, placenta, liver, and spinal cord [3, 60].

GPR37 was initially called endothelin B receptor-like protein because of the significant homology to endothelin-type B (48% similarity and 29% identity) [60]. However, GPR37's closest homolog is the GPR37-like 1 (GPR37L1) with 68% similarity and 48% identity to GPR37 [61] (Figure 4). It has been reported that GPR37 also shares sequence similarity with bombesin receptors (BB_1, and BB_2), another peptide-specific GPCRs [3]. Therefore, it has been suggested that GPR37 can be activated via an endogenous peptide ligand. The first proposed ligand for GPR37 was the invertebrate peptide head activator (HA) [62, 63]. Studies show that HA activates receptor internalization and increases intracellular calcium levels in GPR37-overexpressed heterologous cells [62]. Similarly, HA was also reported to stimulate calcium-mediated nuclear factor of activated T-cell reporter (NFAT) gene transcription and inhibit adenylyl cyclase activity [64].

Several studies tried to replicate HA-mediated receptor activation, but they failed to provide evidence supporting HA as a ligand for GPR37 [65, 66]. The most convincing evidence against HA as a potential ligand for GPR37 is its absence in the human genome, making it unlikely to be GPR37's endogenous ligand [56].

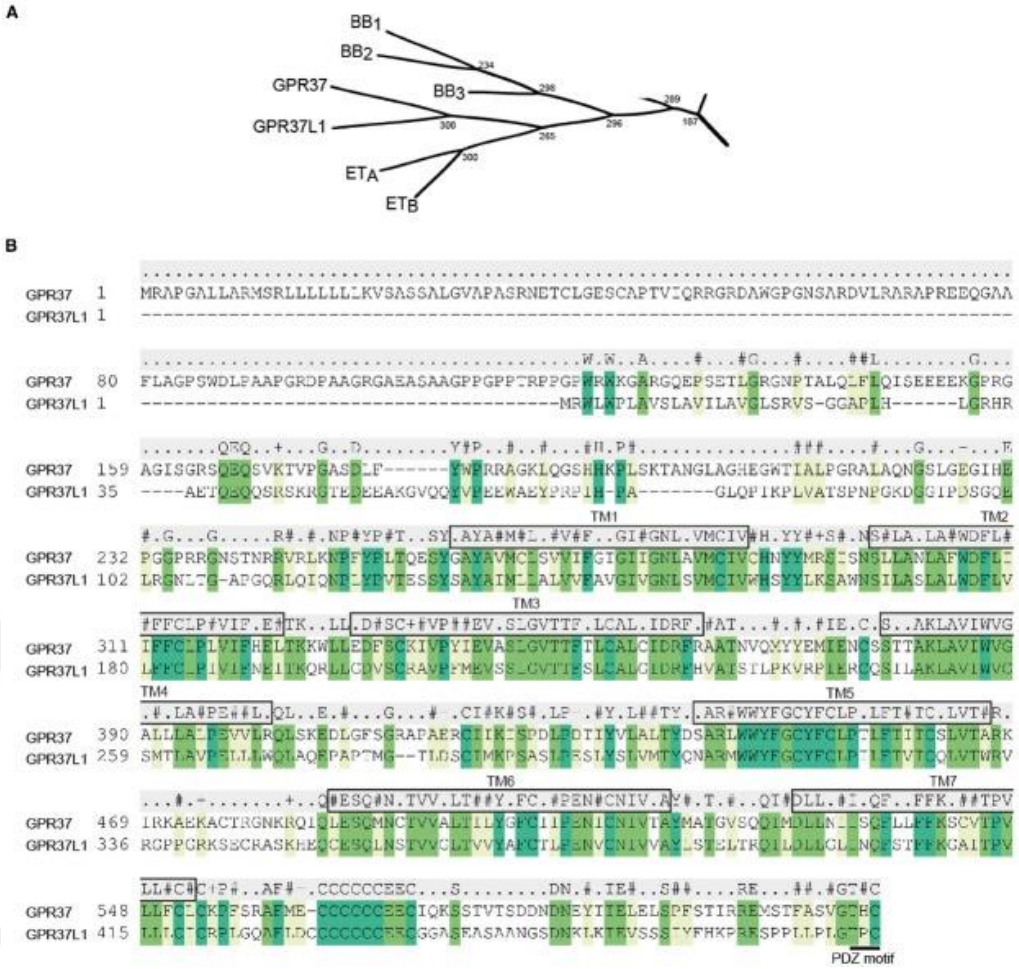

Figure 4. GPR37, GPR37L1, and their closest relatives [67].
A- Phylogenetic relationship between GPR37 and GPR37L1 and the endothelin and bombesin receptors. B- Alignment of human GPR37 and GPR37L1 primary structure highlighting sequence conservation using pairwise alignment. Conserved similarity is indicated for residues that are hydrophobic (#), positively charged (+), negatively charged (–), or unrelated (.). Predicted transmembrane (TM) domains are outlined and labeled.

Another potential ligand for GPR37 is prosaposin (PSAP), a multifunctional protein precursor to four lysosomal activator proteins known as saposin A–D, that promotes the hydrolysis of sphingolipids via lysosomal hydrolases [68]. Full-length prosaposin can also be released into various secretory fluids such as cerebrospinal fluid, milk, pancreatic juice, and bile [69]. The study suggests that prosaposin may have distinct functions beyond its role as a saposin precursor and acts as an extracellular protein. In fact, prosaposin has been recognized as a neurotrophic factor that enhances cell survival, neurite outgrowth, and differentiation [6, 7].

The neurotrophic activity of prosaposin has been attributed to a 12-amino-acid peptide sequence (LIDNNKTEKEIL) located within saposin C region. Furthermore, both saposin C and "prosaptides"—peptides that contain the neurotrophic sequence of prosaposin—have been shown to behave as a neurotrophic factor too. Several prosaptides have been documented in the literature, all of which are variants of prosaposin's peptide sequence that confers its cytoprotective properties [7]. The literature describes various prosaptides, each derived from specific peptide sequences of prosaposin that are responsible for the cytoprotective effects of the full-length prosaposin protein (Figure 5).

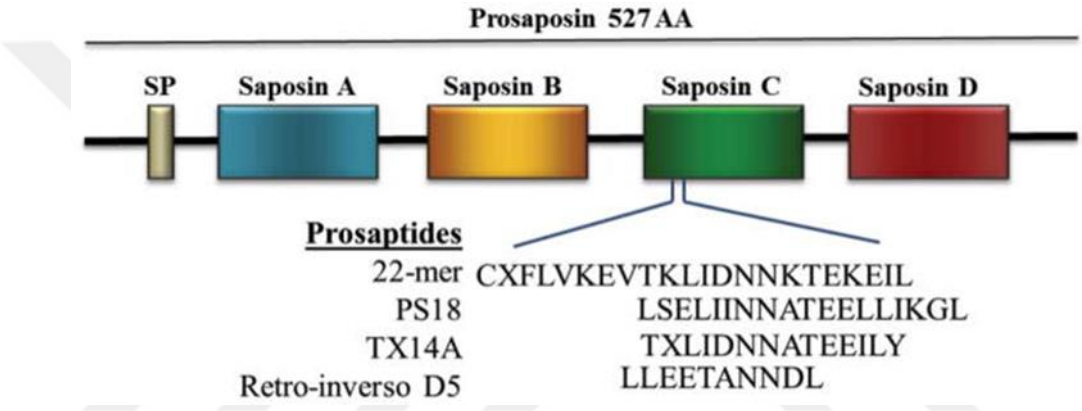

Figure 5. Prosaposin and prosaptides [70].
The Saposin C region promotes the cytoprotective actions of prosaposin. There are several prosaptides derived from this region that will imitate the peptide sequence.

Prosaposin and its derived peptide (synthetic analog), prosaptide TX14(A), have been shown to induce the phosphorylation of extracellular signal-regulated kinases (ERK1 and ERK2) across different cell types. ERK1 and ERK2, essential protein kinases, mediate a range of cellular processes, prominently influencing cell survival through transient activation [71]. For instance, in both primary Schwann cells and an immortalized Schwann cell line, TX14(A) was found to promote ERK phosphorylation, thereby enhancing sulfatide synthesis in Schwann cells [72]. In PC12 cells, prosaposin utilizes ERK phosphorylation to protect the cells against oxidative cell death [73].

Akt, another critical protein kinase, is also known to promote cell survival. Both prosaposin and its prosaptides have been shown to initiate Akt phosphorylation in a variety of cells [74]. In primary Schwann cells, TX14(A) stimulated Akt phosphorylation, supporting Schwann cell survival via the activation of phosphatidylinositide 3-kinases, which act as upstream regulators of Akt [8]. Additionally, prosaposin has been demonstrated to activate the Akt pathway to attenuate oxidative cell death in PC12 cells, alongside its role in the ERK pathway [73].

Recent studies have shown that prosaposin and prosaptide TX14(A) induce ERK1/2 phosphorylation and inhibit forskolin-stimulated cAMP production through GPR37 in GPR37-overexpressed HEK293T cells. To confirm endogenous GPR37 activity, primary cortical astrocytes and siRNA-mediated knockdown of GPR37 are used. While phospho-ERK increased in primary astrocytes via prosaposin or prosaptide TX14(A) treatment, siRNA knockdown of GPR37 reduced this effect. Based on these results, it was concluded that GPR37 was a $G\alpha_i$-coupled receptor [5].

Despite the compelling evidence, the pairing of prosaposin and TX14(A) with GPR37 remains controversial. For instance, the required concentration of prosaptide or TX14(A) for receptor activation (100 nM) is unusually high for peptide-GPCR interactions, which typically occur at much lower concentrations. For example, affinity of ET-1 to ETB receptors is pKd 8.7–9.2 [75]. Questions also arise from discrepancies in ligand-mediated GPR37 internalization. For example, Lundius *et al*. demonstrated, using fluorescence correlation spectroscopy, that GPR37-turboGFP co-localizes with TX14(A) and GM1 gangliosides within lipid rafts in catecholaminergic N2a cells [76]. This interaction suggests a potential protective mechanism involving GPR37, GM1, and lipid rafts against toxic intracellular GPR37 aggregates associated with Parkinson's disease. Furthermore, immunoabsorption of extracellular prosaposin decreased plasma membrane levels of GPR37, which is opposite of the expected outcome of agonist depletion. This finding also contrasts with results of ligand-mediated internalization of GPR37 by prosaposin [5]. Several studies have been unable to replicate the prosaposin/prosaptide-mediated effects on GPR37 signaling. In one

instance, TX14(A) failed to be detected as an agonist for GPR37 in a β-arrestin-based orphan GPCR screen [66]. Another study found that TX14A-activated GPR37 provided protection from oxidative stress in primary astrocytes but failed to observe the same effect in heterologous cells overexpressing the receptor [77]. This inconsistency could imply that the activation of GPR37 might rely on the presence of cell-specific scaffolding proteins or interaction partners. However, further research on the functional relationships between GPR37 and PSAP/TX14A is needed to resolve the discrepancies.

Studies have revealed two additional proposed ligands for GPR37: the bioactive lipid metabolite neuroprotectin D1(NPD1) [78] and the bone-derived protein hormone osteocalcin (OCL) [79]. They are both found to increase intracellular calcium accumulation in GPR37-transfected heterologous cells, as well as peritoneal macrophages for NPD1. In 2021, Bang *et al.* examined the role of GPR37 in models of infection and sepsis, NPD1 demonstrated protective effects against sepsis induced by lipopolysaccharide (LPS) and Listeria in wild-type mice [80]. Notably, these protective effects were absent in GPR37-knockout mice, indicating that GPR37 is crucial for mediating the anti-inflammatory and immune-protective actions of NPD1. In another study, OCL was also found to have protective effects against LPS-caused acute inflammation which were lost in GPR37-knockout mice [81].

Despite the proposal of several ligands for GPR37, none have been officially recognized as endogenous ligands by the IUPHAR yet [82], resulting in GPR37 being classified as an orphan receptor.

GPR37 initially attracted attention as a substrate of parkin, an E3 ubiquitin ligase whose mutated form is directly associated with autosomal recessive juvenile Parkinsonism [9]. Studies have shown that misfolded GPR37 is abundantly present in Lewy bodies, suggesting its potential as a biomarker for Parkinson's disease pathology [83, 84, 10, 85].

Early studies primarily focused on the misfolding of GPR37 and its role in inducing cellular stress, particularly in the absence of parkin or under conditions of receptor overexpression [9, 10, 85]. These conditions are associated with endoplasmic reticulum (ER) stress, which promotes the accumulation and aggregation of misfolded proteins. Misfolded GPR37, unable to be cleared from the cell, forms aggregate that trigger the unfolded protein response, ultimately leading to cell death [9, 86]. While GPR37 overexpression has been associated with cellular toxicity, studies show that GPR37-GFP overexpression can protect N2a cells from dopaminergic toxins like MPP+, rotenone, and 6-OHDA, likely due to increased cell surface expression [87]. This suggests that prosaposin may act as a chaperone for GPR37, ensuring its correct folding and trafficking to the cell surface, where GPR37 signaling could be neuroprotective. Alternatively, prosaposin's neuroprotective effects may be independent of GPR37.

A key challenge in studying GPR37 is its poor trafficking to the plasma membrane and cytotoxicity in most heterologous cell lines. Several strategies have been used to address these issues. Chemical chaperones like 4-phenylbutyrate (4-PBA) have been shown to increase cell surface expression and reduce cytotoxicity in SH-SY5Y neuroblastoma cells [88]. Another approach involved truncating the long GPR37 N-terminus, which restored cell surface expression [65]. Additionally, heterodimerization with other GPCRs, like dopamine D_2 and adenosine A_{2A} receptors or co-expression with interacting partners like the scaffold protein syntenin-1 improved GPR37 trafficking to the plasma membrane [65].

Finally, these findings suggest that although misfolded cytoplasmic GPR37 is toxic, GPR37 localized to the plasma membrane play a cytoprotective role, mediating the neuroprotective effects of secreted prosaposin.

2.6 PI3K/AKT/mTOR Signaling Pathway

The phosphatidylinositol 3-kinase (PI3K)/Akt/mammalian target of rapamycin (mTOR) signaling pathway plays a fundamental role in regulating essential cellular

processes such as cell cycle progression, transcription, translation, differentiation, apoptosis, metabolism, immune function, and cell survival [89]. This cascade is activated by various cell surface receptors, including receptor tyrosine kinases (RTKs) and G protein-coupled receptors [90, 91]. Upon activation, PI3K generates 3'-phosphorylated inositol phosphates, which act as second messengers to recruit and activate downstream effectors, Akt and mTOR (Figure 6).

Akt plays a central role in cell survival by phosphorylating and inhibiting pro-apoptotic factors while activating anti-apoptotic mechanisms [92]. mTOR, downstream of Akt, regulates cellular growth and metabolism through its two distinct complexes, mTORC1 and mTORC2. Among its downstream targets, mTORC1 phosphorylates p70 ribosomal S6 kinase (p70S6K), a key mediator of protein synthesis, ribosome biogenesis and cellular growth. Phosphorylated p70S6K enhances translation by activating ribosomal protein S6 and other components of the translational machinery, thus linking mTOR signaling to cellular growth and metabolic adaptation. The PI3K/Akt/mTOR/p70S6K pathway is critical for cell survival and proliferation, as well as for the regulation of various essential physiological processes [93]. Therefore, dysregulation of this signaling cascade can lead to a variety of pathological conditions, including cancer, neurodegenerative diseases, and immune system dysfunction [94, 95, 96].

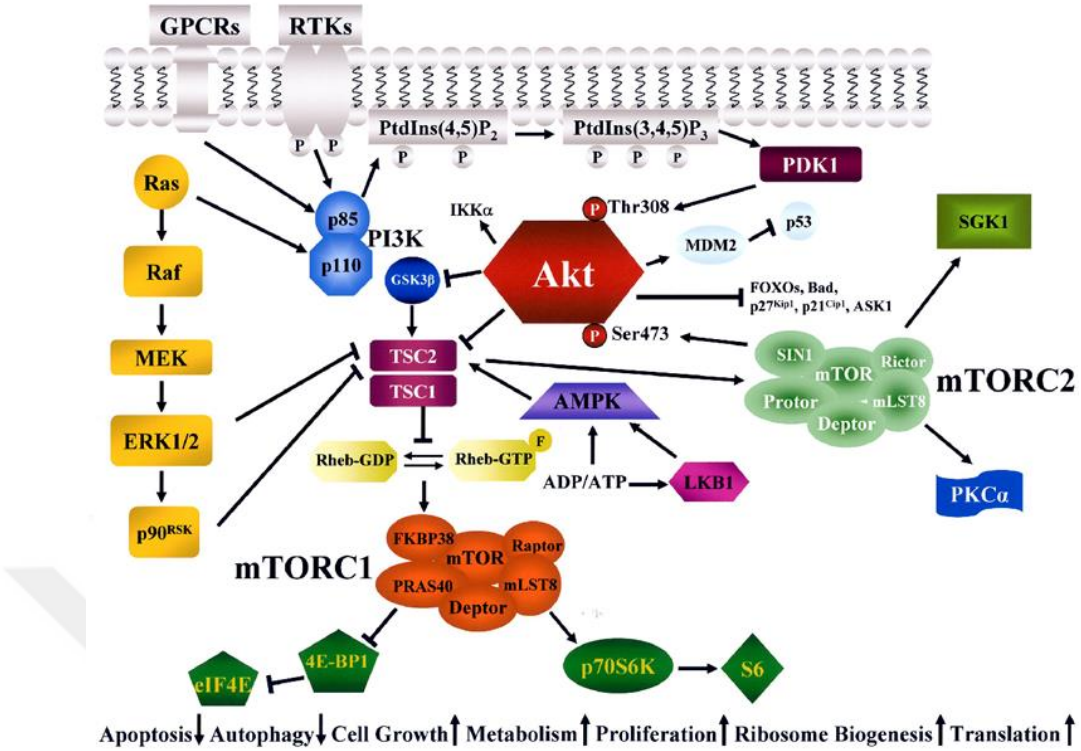

Figure 6. The PI3K/Akt/mTOR signaling pathway [90].
GPCRs, RTKs, and Ras activate the PI3K/Akt/mTOR signaling cascade, which regulates various cellular processes including ribosome biogenesis, cell growth, apoptosis, and metabolism.

Upon ligand binding, GPCRs activate associated G proteins, which initiate a cascade of downstream signaling events through their Gα and Gβγ subunits. Phosphoinositide 3-kinase (PI3K), particularly the isoforms containing p110β or p110γ subunits, is activated by the Gβγ subunit [92]. This triggers the production of phosphatidylinositol 3,4,5-triphosphate (PIP3), a secondary messenger that facilitates the activation of Akt through phosphorylation at specific residues (Thr308 and Ser473). This phosphorylation cascade leads to the full activation of Akt, triggering various downstream signaling events [97]. One of the key roles of Akt is to activate mTOR, a critical regulator of cell growth and protein synthesis. Akt inhibits the TSC1/2 complex, a negative regulator of mTORC1, allowing mTORC1 to activate protein synthesis by phosphorylating key targets such as p70S6K and 4EBP1. By phosphorylating components involved in translation initiation, p70S6K enhances protein production and cell proliferation, making it an essential regulator of cellular responses to growth signals [97].

The activation of the PI3K/Akt/mTOR/p70S6K pathway by GPCRs is influenced by various ligands. These include hormones such as thyroid-stimulating hormone and follicle-stimulating hormone, bioactive lipids like sphingosine 1-phosphate and lysophosphatidic acid, and neurotransmitters like serotonin [98, 99, 100, 101]. These ligands trigger GPCR-mediated signaling, activating PI3K and Akt, which in turn modulate various biological processes such as cell proliferation, survival, and migration. For example, 5-HT can activate the PI3K/Akt pathway via its GPCR, promoting angiogenesis and neuroprotection [101], while the G_i-coupled LPA receptors support cell survival, cell migration, and proliferation via Akt activation [100, 102].

In hepatocellular carcinoma, GPR37 knockdown increases Akt phosphorylation at Ser473, suggesting that suppressing GPR37 may impair cell survival by modulating the PI3K-Akt pathway [103]. In glioma cells, overexpression of GPR37 results in elevated levels of p-AKT (Ser473), providing evidence that upregulation of GPR37 promotes cell survival and proliferation via the PI3K/AKT signaling pathway [104]. In another study, GPR37 was shown to play a significant role in regulating the PI3K/AKT signaling pathway in response to a nutrient stimulus, such as selenomethionine which promotes milk protein and fat synthesis in mammary epithelial cells (MECs) [105]. This nutrient-induced phosphorylation of mTOR and S6K1 is dose-dependent and is blocked after GPR37 knockdown, highlighting its key role in activating the PI3K/AKT/mTOR pathway to regulate cell growth and metabolism in MECs. The involvement of GPR37 in the PI3K/AKT pathway has also been observed in other models. For example, intranasal administration of recombinant PSAP (rPSAP) in ischemic stroke models reduces neuronal apoptosis and promotes cell survival by upregulating the PI3K/Akt/ASK1 pathway. [106].

3 MATERIALS AND METHODS

3.1 Materials

Products and their respective suppliers are shown in Table 1, while Table 2 lists the equipment used in the experiments conducted in this thesis.

Table 1. List of Products and Suppliers

0% Fat Skim milk	Regilait
0.25% Trypsin-EDTA, phenol RED	Gibco
2-mercaptoethanol	Sigma Aldrich
40% Acrylamide/Bis-acrylamide	Serva
Acetic Acid	Sigma Aldrich
Agar	Sigma Aldrich
Amersham Hybond P 0.2 PVDF membrane	GE Healthcare
Amersham Protran 0.2 NC membrane	GE Healthcare
Ammonium persulfate	GE Healthcare
Ampicillin	Sigma Aldrich
Attofluor Cell Chamber	Invitrogen
Bovine Serum Albumin (BSA) Fraction V	Sigma Aldrich
Bradford Reagent, 5x	Serva
Brillant Blue G	Sigma Aldrich
Cell Proliferation Kit	Roche
Dimethyl sulfoxide (DMSO) Hybri-Max	Sigma Aldrich
DMEM, high glucose, non-pyruvate	Gibco
Ditiotreitol (DTT)	Applichem
EDTA-free protease inhibitor cocktail	Roche
Ethanol	Sigma Aldrich
Ethylenediaminetetraacedic acid (EDTA)	Sigma Aldrich
Glycerol	Sigma Aldrich
Glycine	Serva

Table 2. List of Products and Suppliers (continued)

GPR37 (NM_005302) Human Tagged ORF Clone	Origene
HaloTag Alexa Fluor 660 Ligand	Promega
HI Fetal Bovine Serum	Gibco
Hydrochloric acid	Sigma Aldrich
IBIDI μ-Slide 8 Well	Ibidi
Igepal CA-630	Sigma Aldrich
Kanamycin sulfate	Sigma Aldrich
LB Broth	Serva
L-Glutamine	Gibco
Lipofectamine 3000 Transfection Kit	Invitrogen
Methanol	Sigma Aldrich
Mammalian Expression Vector pCMV6-AC-GFP	Origene
Mouse monoclonal anti-B-Actin Antibody (AC-74)	Sigma Aldrich
Mouse monoclonal p-mTOR Antibody (59.Ser 2448): sc-293133	Santa Cruz Biotechnology
Mouse monoclonal p-p70 S6 kinase/S6K1 Antibody (A-6): sc-8416	Santa Cruz Biotechnology
Mouse monoclonal p70 S6 kinase/S6K1 Antibody (H-9): sc-8418	Santa Cruz Biotechnology
Opti-MEM	Gibco
PageRuler™ Plus Prestained Protein Ladder 10 to 250kDa	ThermoFisher Scientific
Pei-MAX	Polysciences
Penicillin-Streptomycin	Gibco
Peroxidase affinipure goat anti-mouse IgG(H+L)	Jackson Immoresearch
Peroxidase affinipure goat anti-rabbit IgG(H+L)	Jackson Immoresearch
Phenylmethanesulfonyl (PMSF)	Applichem

Table 3. List of Products and Suppliers (continued)

Phosphate Buffer Saline (PBS), 1X	Gibco
PI3K/AKT signaling pathway panel	Abcam
Ponceau S	Sigma Aldrich
Potassium Chloride	Sigma Aldrich
Potassium Dihydrogen Phosphate	Sigma Aldrich
Prosaptide TX14(A)	Medchemexpress
Sodium Dodecyl Sulfate (SDS)	Sigma Aldrich
Sodium Azide	Sigma Aldrich
Sodium Chloride	Sigma Aldrich
Sodium Fluoride	Sigma Aldrich
Sodium Hydroxide	Merck
Sodium Orthovanadate	Sigma Aldrich
Sodium Phosphate Dibasic Dodecahydrate	Sigma Aldrich
SuperSignal West Pico Chemiluminescent Substrate	ThermoFisher Scientific
TEMED	Sigma Aldrich
Triton X-100	Sigma Aldrich
Trizma Base	Sigma Aldrich
Trizma Base for Electrophoresis	Serva
Trypan Blue	Sigma Aldrich
Tween 20	Sigma Aldrich
Zymo Pure Midi Prep Kit	ZymoPure
Western Blotting Filter Extra-Thick Paper	ThermoFisher Scientific

Table 4. List of Equipment

-20ºc Freezer	Kirsch
-80ºc Freezer	GLF
4ºc Fridge	Kirsch
Biosafety Cabinet	ThermoFisher Scientific
Cell Culture Incubator	ESCO CCL-170B-8
Chemidoc MP Imaging System	BioRad
Confocal Microscope	Zeiss LSM 700
Confocal Microscope	Zeiss LSM 780
Environmental Shaker/Incubator	ESCO
Flow Cytometer	BD FACSVerse
Inverted Microscope	Zeiss
Micro Centrifuge	ThermoFisher Scientific
Mini Centrifuge	Biosan
Nanodrop	Thermo Scientific One^{C}
Nitrogen Tank	Thermo 30 Thermo Scientific
Plate Reader	BioTek
Trans-Blot Turbo Tranfer System	BioRad
Varioskan Flash	ThermoFisher Scientific
Ventilated Microcentrifuge	ThermoFisher Scientific
Water Bath	St 30 Nüve
Inverted Microscope	Zeiss
Micro Centrifuge	ThermoFisher Scientific
Mini Centrifuge	Biosan
Nitrogen Tank	Thermo 30 Thermo Scientific
Plate Reader	BioTek

3.1.1 Preparation of chemicals, solutions, and buffers

Prosaptide (1mM)

0.001g of prosaptide was dissolved in 633 µl of DMSO to prepare 1 mM main

stocks. The stock solution was filtered with a 0.22 um filter and stored at -80°C.

Protease Inhibitor (PI) (25x)

The Roche cOmplete EDTA-free protease inhibitor cocktail was dissolved in 2 mL of ddH_2O to prepare a 25X stock solution. This stock solution was stored at -20°C. The protease inhibitor was diluted in RIPA buffer for protein isolation to have a final concentration of 1X.

Table 5. 10% Polyacrylamide Separating Gel (1x)

30% Acrylamide/Bisacrylamide	2.66 ml
1.5 M Tris (pH 8.8)	2 ml
50% Glycerol	400 µl
ddH2O	2.85 ml
TEMED	8 µl
10% APS	80 µl

Table 6. 8% Polyacrylamide Separating Gel (1x)

30% Acrylamide/Bisacrylamide	2.12 ml
1.5 M Tris (pH 8.8)	2 ml
50% Glycerol	400 µl
ddH2O	3.4 ml
TEMED	8 µl
10% APS	80 µl

Table 7. 4% Polyacrylamide Stacking Gel (1x)

30% Acrylamide/Bisacrylamide	520 µl
1 M Tris (pH 6.8)	800 µl
20% SDS	32 µl
ddH2O	2560 µl
10% APS	80 µl
TEMED	8 µl

Tris-Glycine running buffer (pH 7.5-8.0), 10x

25 mM Tris

1.92 M Glycine

1% SDS

1X running buffer is diluted from 10X stock with ddH2O

Bjerrum Schafer-Nielsen Transfer buffer, 10x

48 mM Tris

39 mM Glycine

20% methanol

1X transfer buffer is diluted from 10X stock with ddH2O

PBS (pH 7.4), 10x

30 mM KCl

1.37 M NaCl

35 mM KH_2PO_4

100 mM Na_2HPO_4.12H2O

1X PBS is diluted from 10X stock with ddH2O

RIPA lysis buffer, 1x

50 mM Tris-HCl (pH 7.4)

150 mM NaCl

1 mM NaF

1 mM EDTA

1 mM Na_3VO4

0.5 % Igepal CA-630

0.5 % Triton X-100

1 mM DTT

0.5 mM PMSF in EtOH

1% Bromophenol Blue

100mg Bromophenol Blue

10ml methanol

Vortexed and then filtered

Skimmed Milk, 5 %

1X PBS-T is used to prepare 5 % (w/v) skimmed milk

PBST, 1X

1X PBS

% 1 Tween-20

BSA for primary antibodies, 5 %

5 % (w/v) Fraction V BSA 1X PBS

0.02 % NaAzide

Laemmli Sample Buffer, 5X

250mM Tris-HCl (pH 6.8)

5 % SDS

43.5 % Glycerol

0.5 % Bromophenol Blue

Ponceau S

0.1 % (w/v) Ponceau S 5 % Acetic acid

LB Broth (1 Liter)

25 g LB broth was dissolved in 1 liter of ddH_2O and autoclaved.

SOB Medium

2.0% tryptone

0.5% yeast extract

10 mM NaCl

2.5 mM KCl

Autoclaved and added 5 mL of sterile Mg solution per 500 mL

Mg Solution

1 M $MgCl_2$

1 ml $MgSO_4$

Final volume to 500 ml.

CMG Buffer

50 mM $CaCl_2$

50 mM MgCl

16% Paraformaldehyde

16 g PFA

50 ml distilled H_2O

Heat to above 50 °C

Adjust pH until the solution clears.

Final volume to 100 ml.

DTT, 1 M

1.54 g DTT

Distilled H_2O to 10 ml

3.2 Methods

3.2.1 Experimental design

This thesis investigates the function and membrane dynamics of the orphan receptor GPR37 in cellular signaling pathways. HEK293T cells overexpressing GPR37-YFP and GPR37-turboGFP were evaluated for transfection efficiency. The effect of prosaptide on cell viability was assessed using the MTT assay, while Western blotting was performed to analyze the activation of the PI3K/Akt signaling pathway, focusing on the phosphorylation of key downstream proteins. Additionally, prosaptide treatment of GPR37-transfected cells was used to investigate changes in receptor localization and trafficking dynamics. The experimental workflow is shown in Figure 7.

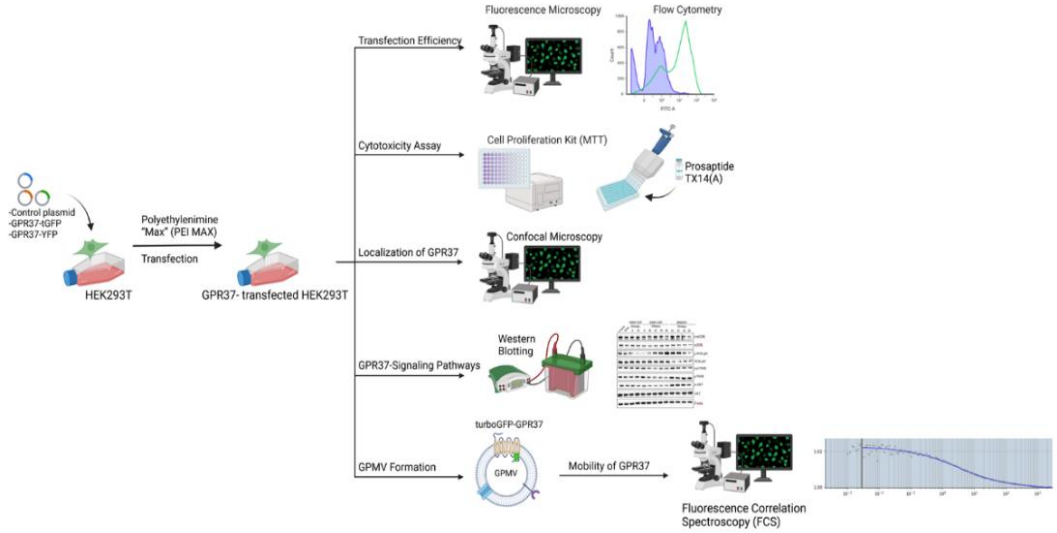

Figure 7. Experimental design of the thesis.

3.2.2 Preparation of chemically competent E. coli and plasmid isolation

5 µl of *E. coli* strain DH5α glycerol stock was mixed with 5 ml LB (liquid broth) and the cells were incubated at 37ºC overnight in a shaker. 1 ml of growth culture was mixed with 100 ml SOB medium and incubated at 37ºC at 200 rpm. The spectrometer at 600 nm followed the culture OD until OD_{600} reached between 0.4-0.6. After the culture was grown to the desired density, it was transferred into sterile 1.5ml centrifuge tubes and centrifuged at 4,000g for 5 minutes at 4 °C. The SOB medium was carefully removed, and the cell pellet was gently resuspended in 30 mL of cold CMG buffer. The suspension was incubated on ice for 15 minutes before being centrifuged again under the same conditions. The supernatant was discarded following centrifugation, and the cells were resuspended in 7.2 mL of cold CMG buffer to ensure proper dispersion. Suspensions were transferred to sterile 1.5 mL centrifuge tubes and incubated on ice for 5 minutes. DMSO was then added in two steps: first, 252 µl was added, mixed thoroughly, and incubated on ice for 5 minutes, followed by the addition of another 252 µl, with the same mixing and incubation. Finally, the prepared cell suspension was aliquoted into sterile microcentrifuge tubes in 100 µl volumes and flash-frozen in liquid nitrogen for storage at -80º C.

GPR37 (NM_005302) Human Tagged ORF Clone (RG208054) and pCMV6-AC-GFP (#PS100010) plasmids were purchased from Origene. GPR37-YFP construct was

kindly gifted by Dr. Francisco Ciruela. For the transformation of these plasmids into DH5α, 2 µl of plasmid was gently mixed with the cells. The mixture was incubated on ice for 30 minutes to allow DNA to bind to the cell membrane. Then cells are placed at 42°C heat block for 45 seconds, followed by immediate cooling on ice for 2 minutes. 900 µl LB medium was added, and the cells were incubated for 1 hour at 37°C with shaking at 200rpm. 100µl of cell suspension was subsequently spread onto LB agar plates containing the appropriate antibiotic (ampicillin or kanamycin) and incubated overnight at 37°C.

A single colony was chosen for plasmid isolation and added into a 100 ml LB medium with the appropriate antibiotic followed by incubation overnight at 37ºC on a 220rpm shaker. ZymoPURE midiprep Plasmid kit was used for the isolation of plasmids. After isolation, concentrations and qualities of plasmids were checked by NanoDrop and by agarose gel electrophoresis (%1 agarose gel). Plasmids were then stored at -80°C.

3.2.3 Cell culture

3.2.3.1 Maintenance of HEK293T cell line

HEK293T human embryonic kidney cells were gifted by Prof. Dr. Eda Tahir Turanlı. The cells were cultured in DMEM high glucose medium supplemented with 1% penicillin/streptomycin and 10% sterile fetal bovine serum (FBS) in a humidified atmosphere of 5% CO2 at 37°C. The cells were maintained in 100 mm cell culture dishes and were passaged twice a week when they reached 80 to 90% confluency. To subculture the cells, the medium was aspirated, and cells were washed with 5 ml 1X PBS without Mg+2 and Ca+2. PBS was aspirated and 1 ml of 0.05% Trypsin/EDTA was added to the cells. After incubation for 3 to 5 minutes, cells were resuspended and collected with 10 ml complete medium in 15 ml tubes and centrifuged at 600 g for 5 minutes at room temperature. The supernatant was aspirated, and the cells were resuspended in 5 ml complete medium. After mixing the cell suspension with trypan blue in a 1:1 ratio, cells were counted by using a hemocytometer.

3.2.3.2 Cryopreservation of the cells

For cryopreservation, cells were grown to approximately 90% confluency in 100 mm culture dishes and were detached from the culture dish as described in the cell line maintenance section. The cell pellet was suspended in a freezing medium composed of 90% DMEM (with 10% FBS) and 10% cell culture grade DMSO. The DMSO was added gradually to the cell suspension after it was resuspended in DMEM with 10% FBS. The final suspension was aliquoted into cryogenic vials, each containing 1 mL of the cell mixture with approximately 2 million cells per vial. Vials were then placed into an into an isopropanol chamber and stored at –80ºC overnight. The next day vials were placed into a nitrogen tank for preservation.

3.2.4 Plasmid transfection

HEK293T cells were seeded in 60mm petri dishes, 25mm coverslips, or ibidi µ-Slide 8 well and transfected with plasmids depending on the experimental setup. The dishes were incubated overnight at 37°C with 5% CO2 for cell attachment. When the cells reached approximately 70% confluency, transfection was initiated.

HEK293T cells were seeded at 0.9 x 10^6 density in 60mm petri dish and were incubated overnight at 5% CO2 at 37°C incubator for cell attachment. For transfection using PEI-Max, 185 µL OPTIMEM was added to two separate microcentrifuge tubes. To one tube, 22.5 µL PEI-Max was added, and to the other, 7.5 µg of plasmid DNA (3:1 PEI-Max to DNA ratio). The tubes were mixed thoroughly and incubated for 30 minutes at room temperature. After incubation, the transfection mixture was added to the cells, and the cells were observed post-transfection using fluorescence microscopy.

For transfection using Lipofectamine 3000, HEK293T cells were seeded in ibidi µ-Slide 8 well at a density of 5 x 10^4 cells per well. Transfection was performed according to the manufacturer's protocol. Briefly, 12.5 µL OPTI-MEM medium was added to two separate tubes. To the first tube, 100 ng plasmid DNA and 0.2 µL P3000 buffer (Lipofectamine 3000) were added and gently mixed. To the second tube, 0.375 µL Lipofectamine 3000 reagent was added and mixed gently. Both solutions were

combined and incubated for 15 minutes at room temperature. The transfection mixture was then added dropwise onto the cells. Cells were observed under fluorescence microscopy within 48 hours after transfection.

3.2.5 Flow cytometry analysis for transfection efficiency

To determine transfection efficiency, HEK293T cells were seeded and transfected with GPR37 (NM_005302) Human Tagged ORF Clone, pCMV6-AC-GFP, and GPR37-YFP in 60 mm dishes, as previously described. Cells were visualized for 48 hours post-transfection to assess transfection efficiency. Following incubation, cells were detached using trypsin, and then centrifuged at 600 g for 5 minutes. The cell pellets were washed with dPBS and centrifuged again at 600 g for 5 minutes to remove the excess medium. The final cell pellets were resuspended in 400 µL dPBS. Cells were counted using a hemocytometer and $3x10^5$ cells from each group were transferred into separate flow cytometry tubes. The samples were analyzed using a BD FACSVerse flow cytometer. A total of 10,000 events were acquired, and the data was properly gated and analyzed with FlowJo software. Non-transfected cell populations were used to define the gate. FITC channel was used to quantify the percentage of transfected cells.

3.2.6 Cell viability assay

HEK293T cells were seeded at a density of 1 x 10^4 cells per well in 96-well plates and incubated for 24 hours at 37°C in a humidified incubator with 5% CO_2. Cells were treated in triplicate with increasing concentrations of prosaptide (0.01 µM, 0.025 µM, 0.05 µM, 0.1 µM, 0.5 µM, 1 µM, 5 µM) for 24 hours. Two controls were included: untreated cells (control cells) and wells containing only medium (blank).

For GPR37-YFP and GPR37-tGFP expressing cells, HEK293T cells were first seeded at a density of 0.9 x 10^6 cells in 60-mm Petri dishes and incubated overnight at 37°C in a humidified incubator with 5% CO_2. Plasmid transfections were performed as described previously. 48 hours after transfection, cells were detached using 0.25% trypsin-EDTA, reseeded at 1 x 10^4 cells per well in 96-well plates, and incubated for

24 hours. Cells were then treated in triplicate with increasing concentrations of prosaptide (0.025 μM, 0.05 μM, 0.1 μM, 0.5 μM, 1 μM) for 24 hours. Three controls were included: untreated cells (control), cells transfected with GFP (mock), and wells containing only medium (blank).

Cell viability was measured using the MTT Cell Proliferation Kit I (Roche) according to the manufacturer's protocol. Briefly, 10 μL of MTT labeling reagent was added to each well and incubated for 4 hours at 37°C. Afterward, 100 μL of solubilization buffer was added to dissolve the formazan crystals, and the plates were incubated overnight. Absorbance was measured at 570 nm using a microplate reader, with a blank reference. Cell viability for treated samples was calculated relative to the untreated control cells, which were defined as 100%.

3.2.7 Protein isolation

HEK293T cells were seeded in 60 mm cell culture dishes, as previously described and transfected with GPR37-tGFP, GPR37-YFP and GFP (control) plasmids. 48 hours after transfection, GPR37-tGFP-expressing cells were treated with 0.1 μM prosaptide for 10, 15, 30, or 60 minutes. GPR37-YFP- and GFP-expressing cells were treated with 0.1 μM prosaptide for 10 minutes. Untreated transfected cells and HEK293T cells were included as controls. At the end of the treatment, the growth medium was aspirated, and cells were collected with 1X cold PBS. Cell pellets were centrifuged at 5000 rpm for 5 minutes at 4°C. After removing supernatants, cell pellets were resuspended in 100μl of 1X RIPA buffer containing 1X protease inhibitors for 30 minutes on ice and vortexed every 10 minutes during incubation. Afterward, suspensions were centrifuged at 14000 g for 15 minutes at 4°C. Supernatants, containing the protein samples, are collected in fresh tubes and were stored at -80°C.

3.2.8 Protein concentration determination

Protein concentrations were determined using Bradford assay. A 5× Bradford stock reagent was diluted with distilled water (ddH_2O) to prepare a 1× working solution. BSA standards were prepared at concentrations of 1.5, 1, 0.75, 0.5, 0.375,

0.25, 0.1875, 0.125, 0.9375 µg/µL from 2 µg/µl BSA. Protein samples were diluted 1:10 with ddH_2O, and 10 µL of each diluted samples and BSA standards were pipetted in triplicate into a 96-well plate. Wells containing 10 µL of ddH_2O served as blanks. To each well, 190 µL of 1× Bradford reagent was added. The plate was incubated in the dark at room temperature for 10 minutes. Following incubation, the absorbance was measured at 595 nm using a microplate reader. Blank absorbance values were averaged and subtracted from the absorbance of the samples and standards. A standard curve was generated using the BSA standards, and the protein concentrations of the samples were calculated based on the linear regression equation derived from the standard curve.

3.2.9 SDS-PAGE and western blotting

Protein samples were prepared by diluting 5X Laemmli sample buffer to 1X with 30 µg protein sample. The final volume of the samples was adjusted to 20 µL with deionized water. All samples were heated at 95° C for 10 minutes to denature the proteins and then placed on ice before loading them into gels. For high molecular weight proteins, 8% acrylamide gel was used, while 10% acrylamide gel was utilized for proteins with lower molecular weights. Electrophoresis was performed at 70V until the samples entered the separating gel, then increased to 110V until the samples reached the bottom. The gels were then transferred to either nitrocellulose or 0.2 µm PVDF membrane using a semi-dry blotting apparatus for 35 minutes at 25V with 1X transfer buffer. For high molecular weight proteins, transfer was carried out in a wet transfer system for 150 minutes at 100V. To confirm successful transfer, membranes were stained with Ponceau S. Excess stain was removed by washing with distilled water. Gels were stained with Coomassie Brilliant Blue to ensure complete transfer and visualize any residual proteins. After transfer, membranes were blocked with 5% skimmed milk in PBST for 1 hour at room temperature to prevent non-specific binding. Membranes were then incubated with rabbit anti-mTOR (1:1000), mouse anti-p-mTOR (1:1000), rabbit anti-akt (1:15000), rabbit anti-p-akt (1:1000), mouse anti-p70S6K (1:1000), mouse anti-p-p70S6K (1:1000), mouse anti-β-actin (1:2000) primary antibodies overnight at 4°C. Next day, membranes were washed three times for 10min with PBST at room temperature and incubated wih horseradish peroxidase

(HRP)-conjugated anti-rabbit (1:1000) or anti-mouse (1:1000) antibodies for 1 hour at room temperature. Membranes were washed three times for 10min with PBST again. To visualize protein bands, membranes were incubated with SuperSignal West Pico chemiluminescent substrate for 2-5 minutes in the dark. Protein bands were imaged using a ChemiDoc imaging system (Bio-Rad) and analyzed with ImageLab software.

3.2.10 Receptor localization by confocal microscopy

HEK293T cells were seeded on 25 mm glass coverslips at density of 2×10^4 cells and allowed to adhere overnight in a humidified incubator at 37°C with 5% CO2. The next day, cells were transfected transfected with GPR37-YFP and GPR37-GFP plasmids using PEI-Max transfection reagent. After 24 hours of incubation, the cells were treated with 1 μM prosaptide and live-cell imaging was performed using Zeiss LSM700 Laser Scanning Microscope equipped with 20x/0.8 Plan-Apochromat and 488 nm laser to excite the plasmids. Prior to imaging, the cells were washed once with pre-warmed PBS to remove residual medium. The medium was then replaced with pre-warmed phenol red-free medium to minimize interference from background fluorescence. Images were captured at the designated time points (20, 30, 40, 50, 60 and 70 minutes) to observe the localization of the receptor and track its dynamics over time. The images were analyzed using Zeiss ZEN software and ImageJ.

3.2.11 GPMV preparation

Giant plasma membrane vesicles (GPMVs) large extracellular vesicles derived from the plasma membrane of living cells through a vesiculation process that involves treatment with paraformaldehyde (PFA) and dithiothreitol (DTT) [107, 108]. This method disrupts cytoskeletal attachments, allowing mobile components of the plasma membrane to separate while leaving cytoskeleton-bound materials behind (Figure 7). As a result, GPMVs maintain the compositional complexity of the native plasma membrane but lack the cortical actin cytoskeleton and intracellular processes, making them an ideal membrane model system for studying membrane protein dynamics in the absence of intracellular trafficking [109, 110].

Cells were grown to ~70% confluence in ibidi chambers and transfected with GPR37-GFP and GFP plasmids using Lipofectamine 3000, as described previously. Twenty-four hours post-transfection, the growth medium was discarded, and the cells were gently washed with HBSS buffer. To induce vesiculation, 1 mL of HBSS buffer, along with 4.5 µL of 16% paraformaldehyde (PFA) stock and 2 µL of 1 M dithiothreitol (DTT), was added to each well, achieving final concentrations of 25 mM PFA and 2 mM DTT. The cells were incubated for 2.5 hours at 37°C in a CO2 incubator. The formation of GPMVs was monitored under a brightfield microscope, where dark vesicles indicated successful vesiculation. The GPMVs were then collected by gently pipetting out the solution. The ibidi chambers were rinsed with 0.1% BSA and washed with HBSS before the GPMV solutions were loaded for further experiments.

3.2.12 Fluorescence correlation spectroscopy (FCS)

Fluorescence Correlation Spectroscopy (FCS) is a technique that offers high spatial and temporal resolution and exceptional sensitivity, used to investigate the molecular dynamics of fluorescent molecules at the single-molecule level by analyzing fluctuations in fluorescence intensity [111, 112]. This makes FCS an invaluable tool for studying GPCR behavior, including receptor interactions, receptor-ligand binding, and the dynamics of receptor signaling [113]. FCS is noninvasive, which is particularly advantageous for examining receptor dynamics in real-time without disrupting the system [114].

Confocal system is used for FCS (Figure 9). FCS is based on the analysis of time correlations in fluorescence fluctuation emitted when fluorescently labeled molecules, such as GPCRs, are diffusing in and out of an observation volume. This analysis offers quantitative information about molecular diffusion (diffusion coefficient), brightness (molecular brightness), and concentration of molecules within the detection volume [112].

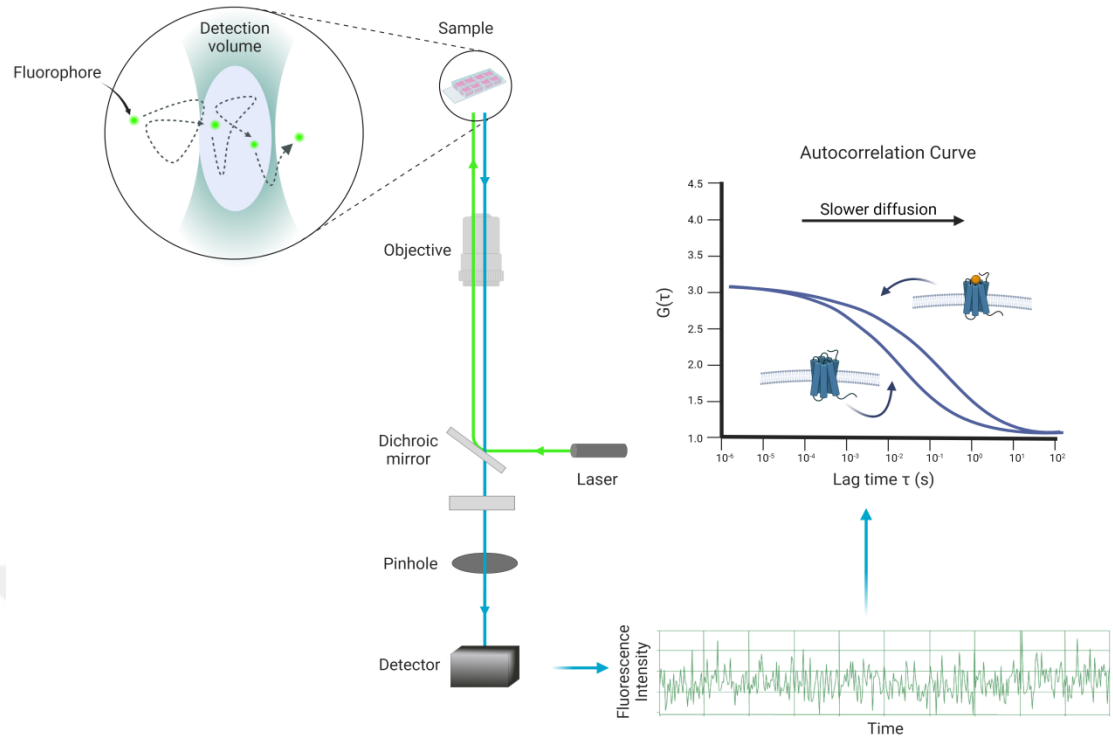

Figure 8. FCS Setup

The autocorrelation function (Gτ) is calculated to know the average dwell time of the fluorescent species in the measurement volume (τ_D), and the average number of particles (N) the autocorrelation curve (Figure 8). The autocorrelation function (Gτ) is given by the equation:

$$G(\tau) = 1 + \frac{\langle \delta I(t)\, \delta I(t+\tau) \rangle}{\langle I(t) \rangle^2}$$

Equation 1 [76].
Where I(t) is the fluorescence intensity at certain time t, and τ is the lag time.

δI(t) = I(t) − <I(t)> is the the difference in fluorescence intensity and the mean fluorescence intensity over the recorded time series is (<I(t)>), and its intensity measured at a later time, $\delta I(t+\tau) = I(t+\tau) - \langle I(t) \rangle$.

The autocorrelation function is influenced by the surrounding environment. For measurements with a single diffusing molecule (tGFP) in cell culture medium, FCS curves were fitted using a model for free three-dimensional (3D) diffusion with

triplet:

$$G(\tau) = 1 + \frac{1}{N} \cdot \left(\sum_i \frac{y_i}{\left(1 + \frac{\tau}{\tau_{Di}}\right)\sqrt{1 + \frac{w_{xy}^2}{w_z^2}\frac{\tau}{\tau_D}}} \right) \cdot \left(1 + \frac{T}{1-T}\exp\left(-\frac{\tau}{\tau_T}\right)\right)$$

Equation 3 [76].

For measurements at the plasma membrane (GPR37-tGFP), FCS curves were fitted using a model for free two-dimensional (2D) diffusion with triplet:

$$G(\tau) = 1 + \frac{1}{N} \cdot \left(\sum_i \frac{y_i}{\left(1 + \frac{\tau}{\tau_{Di}}\right)} \right) \cdot \left(1 + \frac{T}{1-T}\exp\left(-\frac{\tau}{\tau_T}\right)\right)$$

Equation 4 [76].

After obtaining the diffusion time (τ_D), the diffusion coefficient (D) for the lateral mobility of the fluorescent molecule can be calculated using equation 5:

$$D = \omega_0^2 / 4\tau_D$$

Equation 5 where ω is the radius of the confocal detection volume.

GPMVs and live cells were prepared as described previously, with cells seeded and transfected separately with GPR37-GFP and GFP plasmids in Ibidi chambers. FCS experiments were done using a Zeiss LSM 780 confocal microscope equipped with 40× NA 1.2 water immersion objective. Prior to data acquisition, the focal volume was calibrated using a standard solution of 10 nM Alexa Fluor 488 dye to ensure accurate measurements. Calibration was performed at varying laser powers (0.1%, 0.2%, 0.5%, and 1%) to assess the impact of laser intensity on the focal volume and diffusion

parameters. These calibrations also allowed for optimization of the measurement conditions.

FCS measurements were recorded with a 488 nm laser at 0.1% power (~2 μW). FCS measurements were performed on the apical plasma membranes of the cell. The measurements were taken at specific focal spots identified by scanning along the vertical (z) axis, selecting the points with the highest fluorescence intensity. The recorded fluorescence intensity fluctuations were analyzed using FoCuS-point software to fit the FCS curves and determine the diffusion coefficients [115].

3.2.13 Statistical analysis

All data are presented as mean ± standard error of the mean (SEM) unless otherwise specified. Statistical analysis was conducted using GraphPad Prism 5 (GraphPad Software, San Diego, CA, USA). Student's *t*-tests were performed to evaluate the significance of differences. A *p*-value of less than 0.05 was considered statistically significant.

4 RESULTS

4.1 Assessment of Isolated Plasmids

In our study, we used three plasmids: GPR37 (NM_005302) Human Tagged ORF Clone, pCMV6-AC-GFP, and GPR37-YFP construct, which was generously provided by Dr. Francisco Ciruela (Figure 10,11). Each plasmid was isolated using plasmid midiprep to ensure high purity and sufficient yield for subsequent experiments. The quality and concentration of the isolated plasmids were assessed using NanoDrop (Table 7). All plasmids showed high purity, indicated by A260/A280 ratios within the acceptable range (1.8–2.0).

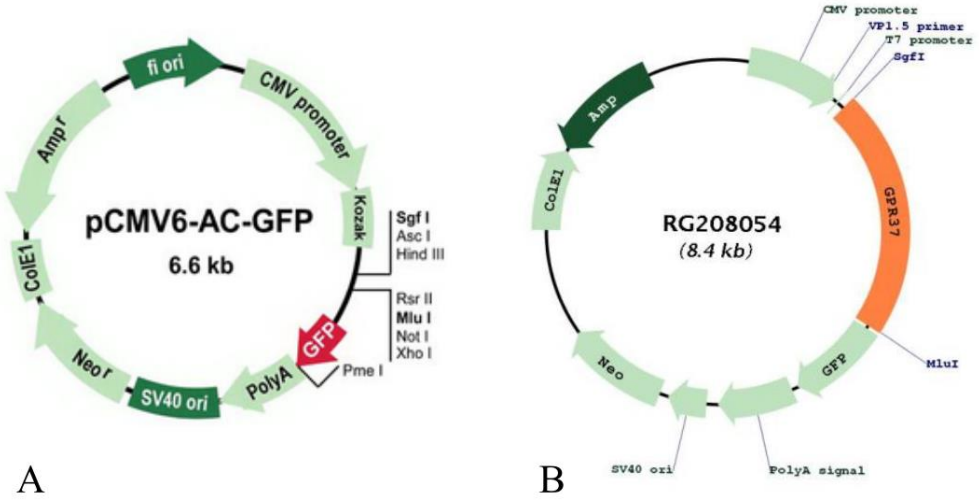

Figure 9. Plasmid maps.
(A) GPR37 (NM_005302) Human Tagged ORF Clone (RG208054) and (B) pCMV6-AC-GFP (#PS100010).

Table 8. Plasmid DNA Concentration

Plasmids	A260/A280	A260/A230	Concentration (ng/ µl)
GPR37 (NM_005302) Human Tagged ORF Clone	1,94	2,37	227,4
pCMV6-AC-GFP	1,89	2,23	91,1
GPR37-YFP	1,89	2,13	77,7

Additionally, the integrity of the plasmids was assessed using 1% agarose gel. The gel analysis revealed distinct bands corresponding to the expected sizes of the plasmids, confirming the successful isolation of intact and uncontaminated DNA.

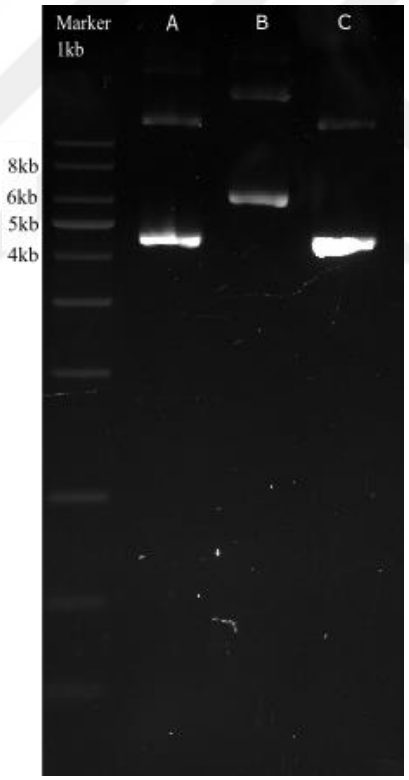

Figure 10. Agarose gel (1%) electrophoresis of isolated plasmids.
(A) GPR37 (NM_005302) Human Tagged ORF Clone, (B) pCMV6-AC-GFP and (C) GPR37-YFP. The first ladder refers to 1kb DNA Marker (NEB).

4.2 Expression of GFP-tagged GPR37 Plasmids in HEK293T Cells

HEK293T cells were transfected using the Polyethylenimine “Max” (PEI MAX) transfection reagent at a 3:1 ratio of PEI to DNA. Transfected cells were examined after 48 hours under a fluorescence microscope to confirm successful transfection and expression of the plasmids (Figure 12).

Polyethylenimine (PEI) is a transfection reagent that binds DNA to form stable, positively charged complexes [116]. These complexes interact with the negatively charged cell surface, allowing cellular uptake through endocytosis. Inside the cell, PEI enables the release of DNA into the cytoplasm by breaking the endosomal membrane. The use of a 3:1 PEI:DNA ratio was optimal for transfecting HEK293T cells with the selected plasmids.

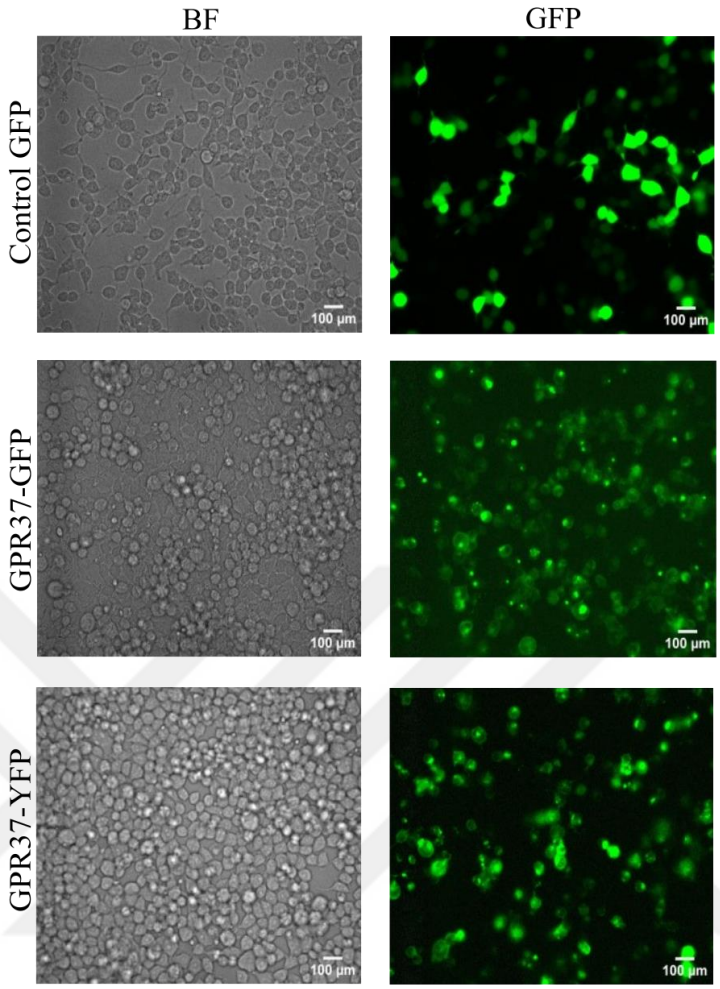

Figure 11. Expression of control (GFP), GPR37-GFP and GPR37-YFP plasmids on HEK293T cells with PEI-MAX.
(Observation of transfected cells on fluorescent microscopy. Cells were transfected at 3:1 ratio (PEI-MAX (µg/ µl): plasmid (µg)) and later they were examined on fluorescent microscopy under the FITC channel with brightfield imaging until 48 hours. Images are taken under 20X magnification. Scale bars were drawn by ImageJ software. (Scale bar, 100 µM.)

4.3 Determination of Transfection Efficiency

To assess the transfection efficiency of our plasmids, we utilized flow cytometry on the FITC channel to detect the GFP signal (Figure 13). This approach allowed us to quantify the percentage of cells expressing fluorescent protein. Before performing subsequent experiments, the transfection efficiency was carefully evaluated. Experiments were only conducted if the transfection efficiency exceeded 50%. The transfection efficiencies, 54% for the control GFP, 65% for GPR37-YFP and 59% for GPR37-GFP, demonstrate the successful introduction of plasmids into HEK293T cells.

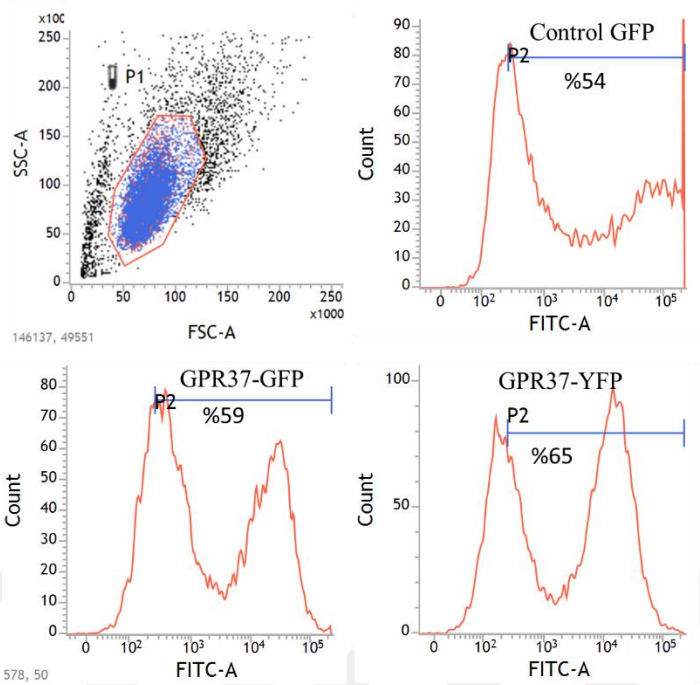

Figure 12. Determination of transfection efficiency with flow cytometry.
(HEK293T cells were transfected with control (GFP), GPR37-GFP and GPR37-YFP plasmids. Non-transfected cells served as a control and were included for gating and population selection during flow cytometry analysis. Cells were harvested by trypsinization and subjected to flow cytometry measurements using the FITC channel to detect fluorescence signals from transfected cells. Control GFP (empty) plasmid had 54%, GPR37-GFP had 59% and GPR37-YFP had 65% efficiency. The BD FACSuite software was used to analyze the data and calculate the proportion of fluorescent cells relative to the non-transfected control group.)

4.4 The Effect of Prosaptide on Cell Viability

The effects of prosaptide treatment on cell viability were evaluated using the MTT assay in both HEK293T cells and HEK293T cells transfected with GPR37-GFP and GPR37-YFP plasmids. Untreated cells served as controls, and non-transfected cells were incubated with increasing concentrations of prosaptide (0.01 µM, 0.025 µM, 0.05 µM, 0.1 µM, 0.5 µM, 1 µM and 5 µM) (Figure 10). For GPR37-transfected cells, prosaptide was given at 0.025 µM, 0.05 µM, 0.1 µM, 0.5 µM, 1 µM concentrations (Figure 14, 15).

The results demonstrated no significant changes in cell viability across all concentrations of prosaptide when compared to the untreated controls. This was consistent in both non-transfected HEK293T cells and those transfected with GPR37-GFP or GPR37-YFP. However, a noticeable difference in cell viability was observed

between transfected and non-transfected cells, likely due to the cytotoxic effects of the transfection agent, PEI-MAX.

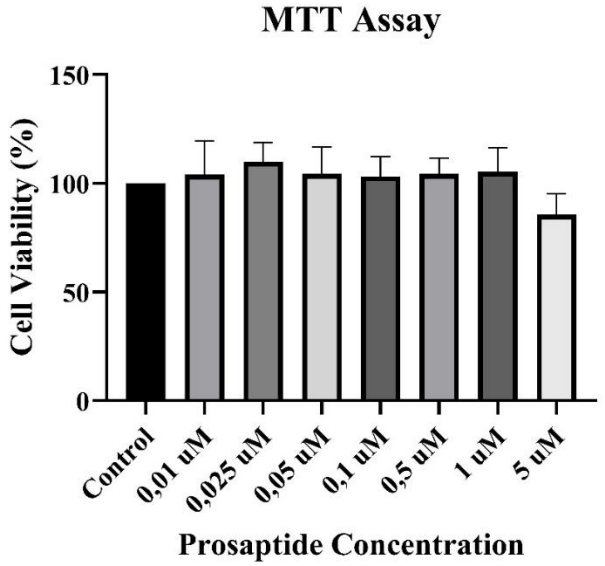

Figure 13. The effect of TX14(A) on cell viability in HEK293T cells.
(HEK293T cells were incubated with different concentrations of prosaptide from 0,01 uM to 5 uM for 24 h. Untreated cells were used as control. The absorbance of the formazan crystals was measured with Varioskan. The bar graph represents the mean ± SEM values of three experiments ($p > 0,05$).)

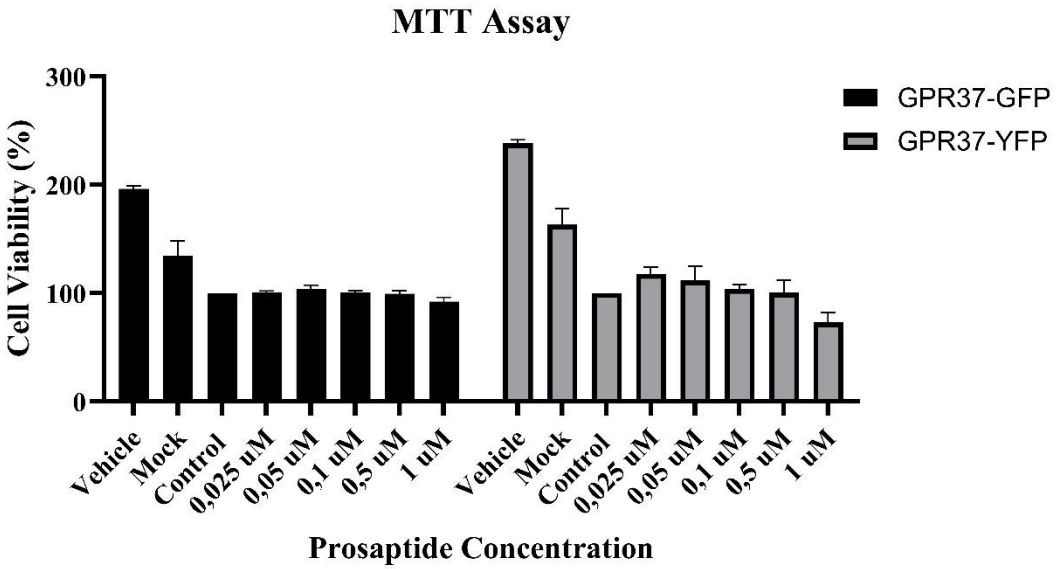

Figure 14. The effect of TX14(A) on cell viability in GPR37-GFP and GPR37-YFP transfected HEK293T cells.
(GPR37-GFP and GPR37-YFP transfected HEK293T cells were incubated with different concentrations of prosaptide from 0,025 uM to 1 uM for 24 h. Untreated transfected cells were used as control. Mock-transfected (GFP) and vehicle-treated non-transfected cells were included as additional controls. The absorbance of the formazan crystals was measured with Varioskan. The bar graph represents the mean ± SEM values of three experiments ($p > 0,05$).)

4.5 GPR37 Localization Upon Prosaptide Treatment

Confocal microscopy was used to investigate the localization of GPR37 in live HEK293T cells transfected with GPR37-GFP and GPR37-YFP plasmids. Fluorescent signals were captured under basal conditions and at various time points (20, 30, 40, 50, 60, and 70 minutes) following treatment with 1 μM TX14(A) (Figure 16).

GPR37 localization was detected at both the plasma membrane and intracellular regions. Over time, changes in the distribution and intensity of fluorescence were observed, with the fluorescent signal progressively shifting from the plasma membrane to intracellular regions, suggesting dynamic alterations in receptor localization following TX14(A) treatment.

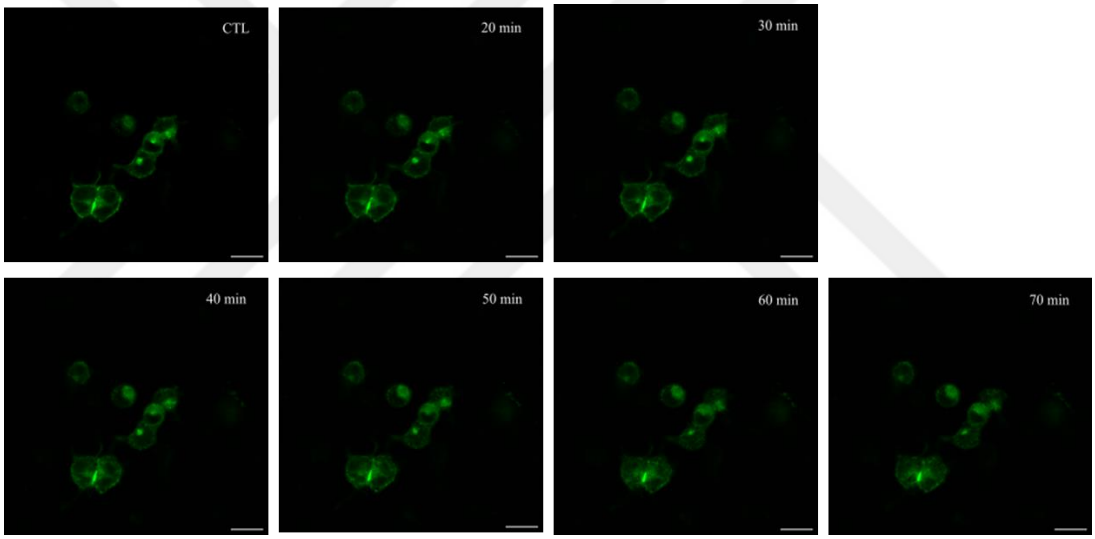

Figure 15. Confocal microscopy images showing the localization of GPR37-GFP in live HEK293T cells.

Localization of GPR37-GFP under basal conditions and at different points (20, 30, 40, 50, 60, and 70 minutes) following TX14(A) treatment. Images were taken with 20x objective using Zeiss LSM 700 confocal microscope and are representative of three independent experiments. Scale bar: 20 μm.

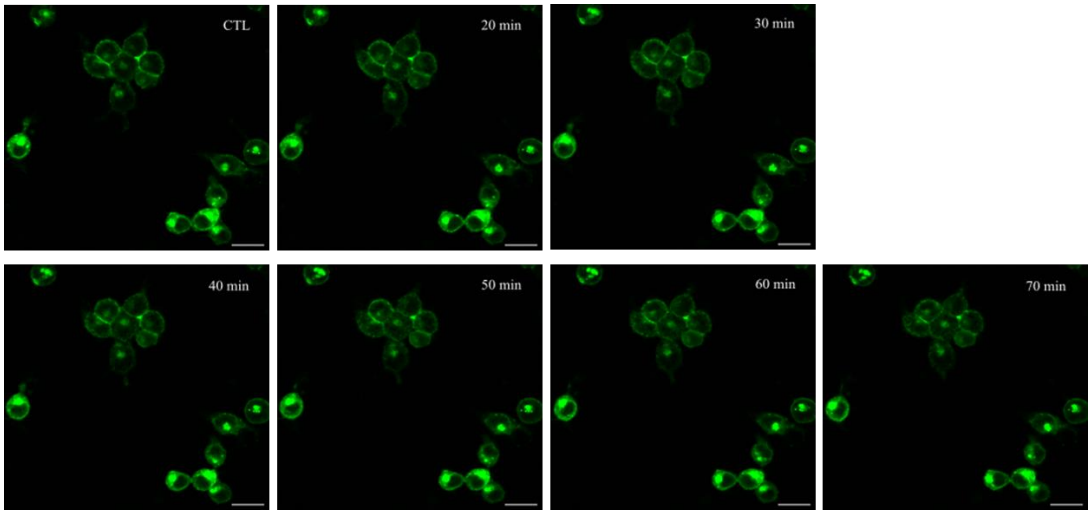

Figure 16. Figure 17. Confocal microscopy images showing the localization of GPR37-YFP in live HEK293T cells.

Localization of GPR37-YFP under basal conditions and at different points (20, 30, 40, 50, 60, and 70 minutes) following TX14(A) treatment. Images were taken with 20x objective using Zeiss LSM 700 confocal microscope and are representative of three independent experiments. Scale bar: 20 μm.

4.6 The Role of GPR37 in PI3K/AKT Signaling Pathway

To assess the downstream effects of GPR37 activation by prosaptide (TX14(A)), key proteins in the PI3K-AKT signaling pathway were analyzed using Western blotting. GPR37-YFP and GPR37-GFP expressing cells and non-transfected HEK293T cells were treated with 0,1 μM TX14(A) for indicated time points (10, 15, 30, 60 minutes), alongside control and mock-transfected (GFP) cells (Figure 17).

While control and mock-transfected cells exhibited minimal changes, GPR37-transfected cells showed increased phosphorylation of PI3K p85, AKT, and mTOR. However, prosaptide treatment did not affect p70S6K phosphorylation. Differences in phosphorylation patterns between GPR37-GFP and GPR37-YFP were also observed. Prosaptide treatment to HEK293T cells increased phosphorylation of AKT.

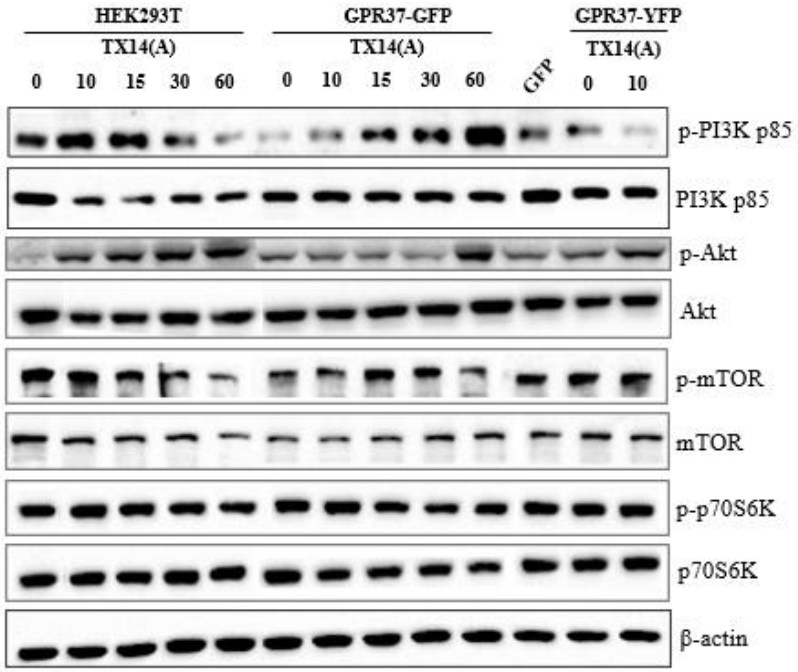

Figure 18. Western blot analysis of the PI3K-AKT-mTOR signaling pathway in GPR37-YFP-expressing, GPR37-GFP-expressing, and non-transfected HEK293T cells treated with 0,1μM TX14(A).
(As indicated, cells were treated for 10, 15, 30, and 60 minutes. Mock GFP and non-transfected untreated cells are used as controls. Western Blot analysis was used to detect protein levels and β-Actin was used as a loading control)

4.7 Diffusion Dynamics of GPR37

To investigate the photophysical behaviors of turboGFP and eGFP, with a particular focus on turboGFP due to its use in subsequent experiments involving GPR37-turboGFP, their diffusion properties were evaluated under varying laser power intensities using FCS (Figure 18). Diffusion coefficients for turboGFP increased significantly with laser power intensity, from 25.89 μm²/s at 0.1% to 72.53 μm²/s at 1%. In contrast, eGFP diffusion coefficients remained stable, ranging between 31.42 μm²/s and 37.66 μm²/s across all laser powers. For GPR37-turboGFP, the 1% laser intensity was excluded due to its high laser power, and an additional lower intensity of 0.05% was introduced to optimize the investigation of diffusion dynamics of GPR37-turboGFP expressing HEK293T cells.

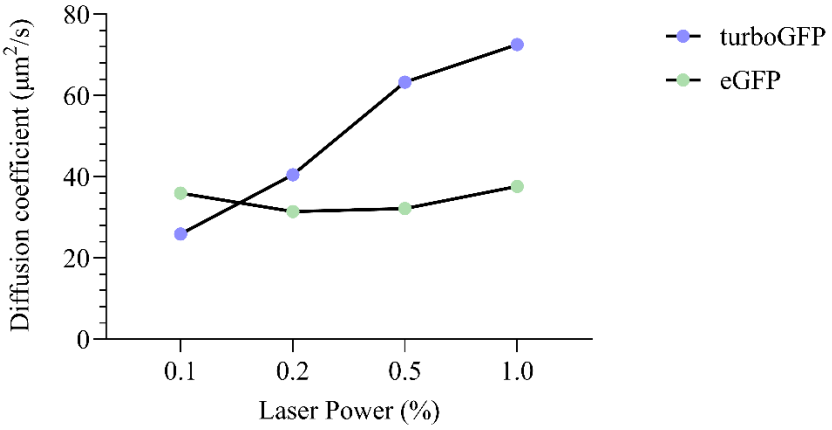

Figure 19. Diffusion coefficient of turboGFP and eGFP under varying laser powers (% of the full power).
(HEK293T cells are transfected with turboGFP and eGFP plasmids and incubated at 30°C 5% CO_2 for 24h before performing FCS measurements. Excitation was achieved using a 488 nm laser. Laser power intensities were adjusted to 0.1%, 0.2%, 0.5% and 1% of the total power output. Autocorrelation functions were recorded for each condition and fitted to a 3D diffusion model with triplet to calculate diffusion coefficients (D)).

To investigate the diffusion properties of GPR37-turboGFP compared to turboGFP in solution, FCS was performed at varying laser power intensities (0.05%, 0.1%, 0.2%, and 0.5%) (Figure 19). For turboGFP, the diffusion coefficients were consistent at lower laser powers (0.05% and 0.1%). However, a substantial increase was observed at higher laser powers (0.2% and 0.5%). In contrast, GPR37-turboGFP displayed considerably lower diffusion coefficients across all laser intensities, which is consistent with the behavior of membrane-bound GPCRs, although the observed diffusion coefficients were somewhat higher than anticipated (Figure 20). Specifically, at 0.05%, the diffusion coefficients were 2.98μm²/s and 7.94 μm²/s, and at 0.1%, they increased slightly to 4.56μm²/s and 9.70μm²/s. At 0.2% and 0.5%, the diffusion coefficients increased, although they remained significantly lower than those for turboGFP.

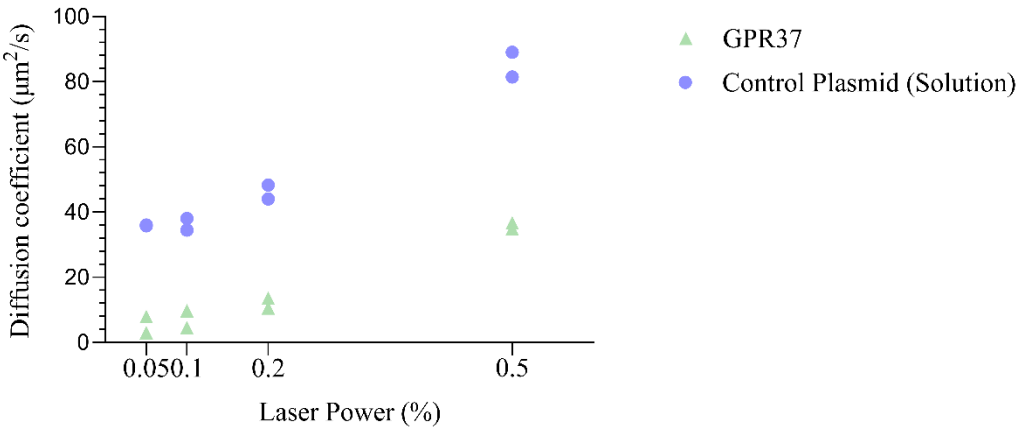

Figure 20. Diffusion coefficient of GPR37-turboGFP and turboGFP under varying laser powers (% of the full power).

(HEK293T cells are transfected with turboGFP and GPR37-turboGFP plasmids and incubated at 30°C 5% CO_2 for 24h before performing FCS measurements. Excitation was achieved using a 488 nm laser. Laser power intensities were adjusted to 0.05%, 0.1%, 0.2% and 0.5% of the total power output. Autocorrelation functions were recorded for each condition and fitted to a 2D diffusion model with triplet for GPR37-turboGFP and to a 3D diffusion model with triplet for turboGFP to calculate diffusion coefficients (D). Two independent experiments are done).

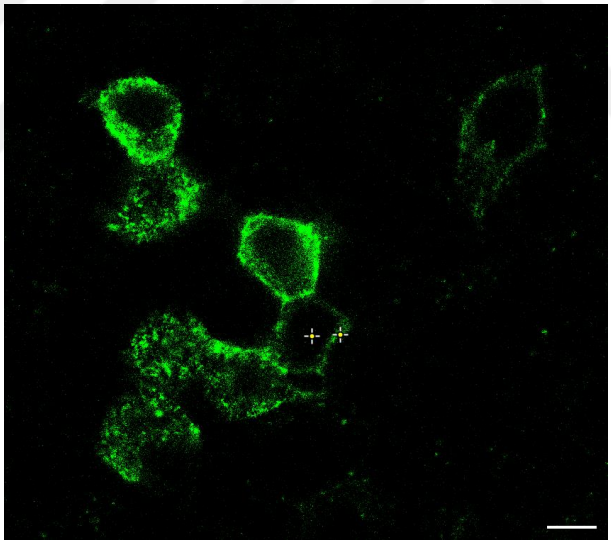

Figure 21. Confocal microscopy image of GPR37-turboGFP transfected HEK293T cells.

Live-cell fluorescence images were used to localize the confocal observation volume above the cell nucleus (indicated by a cross). A cross indicated the plasma membrane. Scale bar = 10 μm.

4.8 Molecular Mobility of GPR37 in GPMVs

HEK293T cells were transfected with GPR37-turboGFP and turboGFP plasmids, followed by GPMV preparation to investigate the diffusion properties of GPR37 in the membrane environment of GPMVs. The diffusion coefficients of

GPR37-GFP in GPMVs were measured and compared to turboGFP in solution as a control. The diffusion coefficients for GPR37-GFP in GPMVs ranged from 1.79 to 8.77 µm²/s, significantly lower than the 82 to 106 µm²/s observed for turboGFP (Figure 22.A). Additionally, brightfield images of GPMVs transfected with GPR37-turboGFP showed successful vesiculation with dark vesicular structures, while confocal images demonstrated the fluorescence of GPR37-turboGFP (Figure 21).

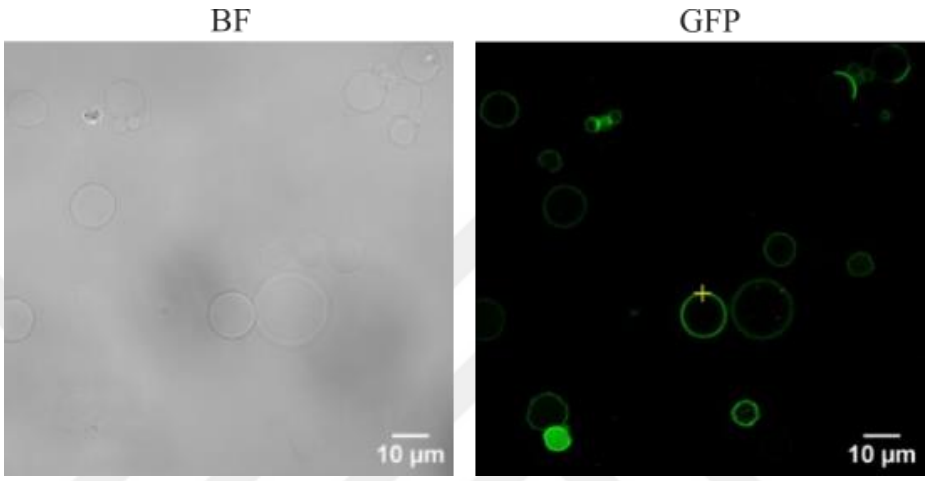

Figure 22. Confocal microscopy image (GFP) and brightfield image (BF) of GPR37-turboGFP transfected GPMVs.
A cross indicates the plasma membrane where FCS measurements are performed. Scale bar = 10 µm.

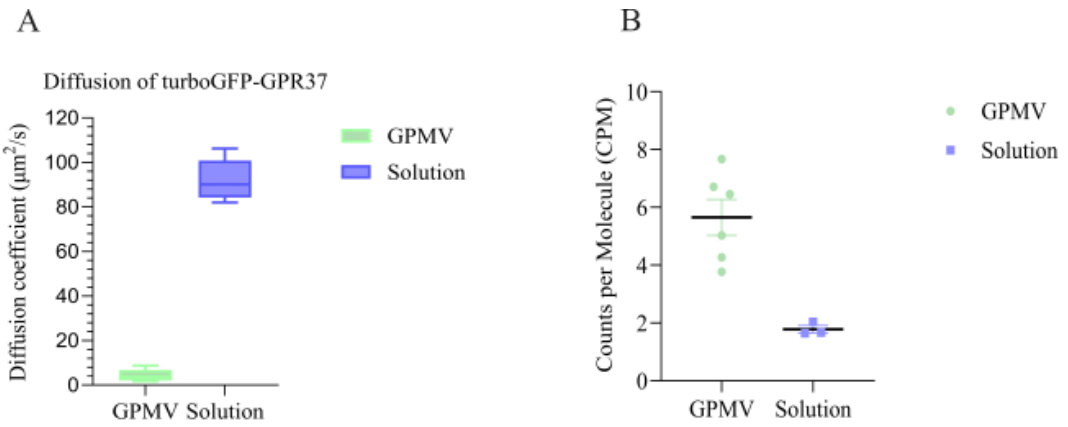

Figure 23. Diffusion of GPR37-turboGFP in GPMVs.
((A) Diffusion coefficient of GPR37-turboGFP and turboGFP in GPMVs. (B) Count per molecule (CPM) for GPR37-turboGFP and turboGFP. HEK293T cells are transfected with turboGFP and GPR37-turboGFP plasmids and incubated at 30°C 5% CO2 for 24h before GPMV preparation. For FCS measurements, 488 nm laser is used for fluorescence excitation. Laser power intensities were adjusted to 0.1%. Autocorrelation functions were recorded for each condition and fitted to a 2D diffusion model with triplet for GPR37-turboGFP and to a 3D diffusion model with triplet for turboGFP to calculate diffusion coefficients (D). Two independent experiments are done)

The count per molecule (CPM) values for GPR37-turboGFP in GPMVs were between 3.77 kHz and 6.71 kHz, significantly higher than those observed for turboGFP, which were between 1.64 kHz and 2.03kHz (Figure 22.B). These higher CPM values for GPR37-turboGFP in GPMVs suggest that the receptor may experience clustering or interactions that enhance the fluorescence signal, potentially due to oligomerization or other membrane-associated behaviors.

5 CONCLUSION

GPCRs constitute the largest family of membrane receptors involved in cellular signal transduction [1]. GPCRs mediate diverse physiological processes via ligand binding, receptor activation and triggering downstream signaling pathways [13]. Among them, GPR37 is of particular interest due to its relation to Parkinson's disease and its emerging role in neuroprotection and cellular stress responses [3, 4]. Although GPR37 is categorized as orphan GPCR due to the absence of a known endogenous ligand, several studies have proposed multiple ligands such as HA, OCL and NPD1 [4]. Among these, prosaposin and synthetic peptides derived from the active neurotrophic domain of prosaposin, prosaptide, have been identified as promising ligands for GPR37 [70]. Prosaptide, particularly TX14(A) demonstrated the ability to activate pathways like ERK1/2 and Akt, contributing to cell survival and protective effects in various cell types, such as Schwann cells and PC12 cells [8, 72]. The PI3K-AKT pathway is widely known for its involvement in regulating cell growth, survival, and metabolism [89]. However, prosaptide interaction with GPR37 remains questionable due to the high concentrations required for receptor activation and inconsistencies in ligand-mediated receptor internalization [75, 76].

In this study, we investigated the role of the PI3K-AKT-mTOR pathway in GPR37 activation by prosaptide TX14(A) to understand the signaling mechanisms related to GPR37. For this purpose, HEK293T cells were transfected with GPR37-YFP, GPR37-GFP and control (GFP) plasmids. After confirming successful transfections through fluorescence microscopy, the transfection efficiency was further assessed using flow cytometry. To determine the optimal concentration of prosaptide for our experiments, we tested various concentrations (0.01 μM to 5 μM) in HEK293T cells and GPR37-transfected HEK293T cells using the MTT assay to evaluate cell viability. The results revealed no significant changes in cell viability at any of the concentrations, indicating that prosaptide does not induce cytotoxicity under the conditions tested. Given that 0.1 μM was used in previous studies, we selected 0.1 μM for further experiments to investigate its effects on signaling pathways.

Confocal microscopy was used to examine the localization of GPR37-GFP and GPR37-YFP in live HEK293T cells, both under basal conditions and after treatment with TX14(A) at multiple time points (20, 30, 40, 50, 60, and 70 minutes). The fluorescence signal, which initially localized at the plasma membrane, gradually shifted to intracellular regions over time. This dynamic redistribution of fluorescence suggests that TX14(A) may induce changes in GPR37 localization, possibly due to receptor internalization, a key feature often associated with GPCR activation. Our findings also showed a more detectable shift in GPR37-GFP fluorescence localization compared to GPR37-YFP following TX14(A) treatment. Structural or folding differences between GFP and YFP may have influenced the receptor's behavior, and variations in expression levels could have further impacted the results. Also, in heterologous cell lines, overexpression of receptors can lead to altered trafficking pathways or receptor accumulation in intracellular compartments, which could obscure the clear visualization of receptor internalization.

Our study aimed to explore the downstream effects of GPR37 activation by prosaptide on the PI3K-AKT-mTOR signaling pathway. While control and mock-transfected cells exhibited minimal changes in phosphorylation, GPR37-expressing cells showed an increased phosphorylation of PI3K p85, AKT, and mTOR. However, prosaptide treatment did not alter p70S6K phosphorylation, suggesting that GPR37 activation may regulate key signaling molecules within the pathway without strongly impacting its downstream effector S6K1.

Interestingly, differences in phosphorylation patterns were observed between GPR37-GFP and GPR37-YFP, which may indicate structural or functional variations between these tagged receptor variants. Additionally, prosaptide treatment in HEK293T cells led to increased AKT phosphorylation, suggesting that prosaptide may activate AKT signaling through endogenous receptors or alternative pathways independent of GPR37. These findings highlight the complexity of GPR37's role in PI3K-AKT-mTOR signaling and raise important questions about its specific regulatory mechanisms.

The observed differences between the GPR37-GFP and GPR37-YFP expressing cells further complicate the interpretation of these results. The distinct phosphorylation patterns between these two tagged versions of GPR37 could suggest that the tagging itself may influence receptor activation or downstream signaling events. These discrepancies highlight the complexity of GPR37 signaling and suggest that further investigation is needed to elucidate the precise mechanisms through which prosaptide modulates the PI3K-AKT-mTOR pathway and its impact on cellular responses such as survival, growth, and metabolism. Additional studies, including those focusing on the potential role of scaffolding proteins and cell-type specific properties, will be necessary to resolve the observed inconsistencies and fully understand the functional implications of GPR37 activation in different contexts.

FCS was utilized to measure the diffusion coefficients of GPR37 under varying laser intensities, providing a high-resolution approach to study molecular mobility. Our results demonstrate a clear contrast in the diffusion properties of turboGFP and eGFP. While the diffusion coefficient of turboGFP increased significantly with higher laser intensities, ranging from 25.89 $\mu m^2/s$ at 0.1% to 72.53 $\mu m^2/s$ at 1%, eGFP diffusion remained stable at values between 31.42 $\mu m^2/s$ and 37.66 $\mu m^2/s$. This discrepancy suggests that turboGFP is more susceptible to changes in laser power, while diffusion of eGFP is relatively unaffected by variations in laser intensity. The stable diffusion behavior of eGFP makes it a reliable probe in scenarios where consistent diffusion is required.

Observed diffusion coefficients for GPR37, although lower than those for turboGFP (control), were still higher than expected for membrane-bound GPCRs, which typically range from 0 to 1 $\mu m^2/s$. This suggests that while GPR37 is membrane-localized GPCR, it may not be as tightly restricted. Several factors could contribute to this increased mobility, including weak interactions with cytoskeletal components or an altered membrane microenvironment. Overexpression of GPR37 may result in inefficient trafficking to the plasma membrane, with some of the receptors retained in intracellular compartments such as the ER or vesicles, leading to higher-than-expected diffusion coefficients [9]. These observations emphasize the complexity of membrane-

bound receptor dynamics, where various factors beyond simple membrane tethering can influence diffusion characteristics.

To further investigate the membrane-specific dynamics, GPMVs were used, showing significantly lower diffusion coefficients for GPR37-turboGFP. In cells, GPCRs experience various intracellular constraints, such as interactions with the cytoskeleton, intracellular trafficking, and potential clustering at lipid rafts or other microdomains. These factors affect their lateral mobility within the membrane. In GPMVs, while the complex intracellular environment is removed, the proteins are still confined to a lipid bilayer, which mimics the plasma membrane but lacks other intracellular structures. Our findings were further supported by FCS measurements in GPMVs, which closely mimic the natural cellular environment of GPR37. GPR37-turboGFP showed diffusion coefficients ranging from 1.79 $\mu m^2/s$ to 8.77 $\mu m^2/s$, much lower than the 82 $\mu m^2/s$ to 106 $\mu m^2/s$ observed for turboGFP in solution. This difference highlights the profound effect that the membrane association has on the diffusion of GPR37, further emphasizing the restricted movement of membrane-bound receptors. The significantly higher count per molecule (CPM) values for GPR37-turboGFP (3.77 kHz to 6.71 kHz) compared to turboGFP (1.64 kHz to 2.03 kHz) in GPMVs suggest that GPR37 may undergo clustering or oligomerization in the membrane, which would enhance the fluorescence signal and may be indicative of protein-protein interactions or receptor aggregation. This clustering could also influence the receptor's functionality, as oligomerization is a well-known mechanism through which GPCRs modulate signaling pathways.

6 CONCLUSION

GPCRs such as GPR37 play a pivotal role in cellular signaling by undergoing complex conformational changes and internalization processes following ligand binding. This study demonstrates that prosaptide activation of GPR37 significantly alters the PI3K-AKT pathway, as evidenced by increased phosphorylation of PI3Kp85, Akt and mTOR. These results suggest that GPR37 plays a role in regulating cellular signaling pathways, which could influence cell survival, metabolism, and overall cellular function. Furthermore, the localization of GPR37 reveal that, upon prosaptide treatment, GPR37 undergoes a shift from the plasma membrane to intracellular compartments, indicating receptor internalization.

The diffusion dynamics of GPR37 in the membrane were significantly different in cells and GPMVs. In cells, GPR37 exhibited higher diffusion coefficients. This discrepancy could be attributed to the challenges in accurately capturing the movement of GPR37 in the complex cellular environment, where the receptor may be trapped in intracellular compartments such as the ER or vesicles, limiting its membrane-associated diffusion. Conversely, GPR37 in GPMVs demonstrated lower diffusion coefficients, closer to the expected behavior of membrane proteins in a less complex, model membrane environment. This comparison emphasizes how cellular complexity, and intracellular structures can limit the mobility of membrane receptors.

Overall, these findings suggest that GPR37 exhibits complex diffusion dynamics, intracellular trafficking, and signaling behavior. Prosaptide activation provides insights into its potential role in modulating key signaling pathways, though further studies are required to fully elucidate its biological functions and therapeutic applications.

7 REFERENCES

1. Rosenbaum DM, Rasmussen SG, Kobilka BK. The structure and function of G-protein-coupled receptors. Nature. 2009; 459(7245):356-363.
2. Laschet C, Dupuis N, Hanson J. "The G protein-coupled receptors deorphanization landscape." Biochemical Pharmacology. 2018;153:62-74.
3. Marazziti D, Golini E, Gallo A, Lombardi MS, Matteoni R, Tocchini-Valentini GP. Cloning of GPR37, a gene located on chromosome 7 encoding a putative G-protein-coupled peptide receptor, from a human frontal brain EST library. Genomics. 1997; 45(1):68-77.
4. Bolinger AA, Frazier A, La JH, Allen JA, Zhou J. Orphan G protein-coupled receptor GPR37 as an emerging therapeutic target. ACS Chemical Neuroscience. 2023;14(18):3318–3334.
5. Meyer RC, Giddens MM, Schaefer SA, Hall RA. GPR37 and GPR37L1 are receptors for the neuroprotective and glioprotective factors prosaptide and prosaposin. Proceedings of the National Academy of Sciences of the United States of America. 2013; 110(23):9529-9534.
6. O'Brien JS, Carson GS, Seo HC, Hiraiwa M, Kishimoto Y. Identification of prosaposin as a neurotrophic factor. Proceedings of the National Academy of Sciences of the United States of America. 1994; 91(20):9593-9596.
7. O'Brien JS, Carson GS, Seo HC, Hiraiwa M, Weiler S, Tomich JM, Barranger JA, Kahn M, Azuma N, Kishimoto Y. Identification of the neurotrophic factor sequence of prosaposin. FASEB journal: official publication of the Federation of American Societies for Experimental Biology. 1995; 9(8):681-685.
8. Campana WM, Darin SJ, O'Brien JS. Phosphatidylinositol 3-kinase and Akt protein kinase mediate IGF-I- and prosaptide-induced survival in Schwann cells. Journal of Neuroscience Research. 1999;57(3):332–341.
9. Imai Y, Soda M, Inoue H, Hattori N, Mizuno Y, Takahashi R. "An unfolded putative transmembrane polypeptide, which can lead to endoplasmic reticulum stress, is a substrate of Parkin." Cell. 2001;105(7):891-902.
10. Kitao Y, Imai Y, Ozawa K, Kataoka A, Ikeda T, Soda M, Nakimawa K, Kiyama H, Stern DM, Hori O, Wakamatsu K, Ito S, Itohara S, Takahashi R, Ogawa S. "Pael receptor induces death of dopaminergic neurons in the substantia nigra via endoplasmic reticulum stress and dopamine toxicity, which is enhanced under condition of parkin inactivation." Human Molecular Genetics. 2007;16(1):50-60.
11. Gerstle Z, Desai R, Veatch SL. "Giant Plasma Membrane Vesicles: An Experimental Tool for Probing the Effects of Drugs and Other Conditions on Membrane Domain Stability." Methods in Enzymology. 2018;603:129-150.
12. Fredriksson R, Lagerström MC, Lundin LG, Schiöth HB. "The G-protein-coupled receptors in the human genome form five main families. Phylogenetic analysis, paralogon groups, and fingerprints." Molecular Pharmacology. 2003;63(6):1256–1272.

13. Morris AJ, Malbon CC. Physiological regulation of G protein-linked signaling. Physiological reviews. 1999; 79(4):1373-1430.
14. Wettschureck N, Offermanns S. Mammalian G proteins and their cell type specific functions. Physiol Rev, 2005; 85(4):1159-204
15. Kobilka BK. "G protein coupled receptor structure and activation." Biochimica et Biophysica Acta. 2007;1768(4):794-807.
16. Patel TB. Single transmembrane spanning heterotrimeric g protein-coupled receptors and their signaling cascades. Pharmacological reviews. 2004; 56(3):371-385.
17. Pierce KL, Premont RT, Lefkowitz RJ. Seven-transmembrane receptors. Nature reviews. Molecular cell biology. 2002; 3(9):639-650.
18. Marinissen MJ, Gutkind JS. G-protein-coupled receptors and signaling networks: emerging paradigms. Trends in pharmacological sciences. 2001; 22(7):368-376.
19. Heng BC, Aubel D, Fussenegger M. "An overview of the diverse roles of G-protein coupled receptors (GPCRs) in the pathophysiology of various human diseases." Biotechnology Advances. 2013;31(8):1676-1694.
20. Rehman S, Rahimi N, Dimri M. Biochemistry, G Protein Coupled Receptors. StatPearls Publishing, 2023.
21. Thompson MD, Cole DE, Capra V, Siminovitch KA, Rovati GE, Burnham WM, Rana BK. Pharmacogenetics of the G protein-coupled receptors. Methods Mol Biol, 2014; 1175:189-242.
22. Overington JP, Al-Lazikani B, Hopkins AL. How many drug targets are there? Nature reviews. Drug discovery. 2006; 5(12):993-996.
23. Bockaert J. Les récepteurs couplés aux protéines G - Prix Nobel de chimie 2012 Robert J. Lefkowitz et Brian Kobilka. [G-protein coupled receptors. Nobel Prize 2012 for chemistry to Robert J. Lefkowitz and Brian Kobilka] Médecine Sciences. 2012;28(12):1133–1137.
24. Lin HH. "G-protein-coupled receptors and their (Bio) chemical significance win 2012 Nobel Prize in Chemistry." Biomedical Journal. 2013;36(3):118-124.
25. Kolakowski LF Jr. "GCRDb: a G-protein-coupled receptor database." Receptors & Channels. 1994;2(1):1-7.
26. Probst WC, Snyder LA, Schuster DI, Brosius J, Sealfon SC. Sequence alignment of the G-protein coupled receptor superfamily. DNA and cell biology. 1992; 11(1):1-20.
27. Alexander SP, Christopoulos A, Davenport AP, Kelly E, Marrion NV, Peters JA, Faccenda E, Harding SD, Pawson AJ, Sharman JL, Southan C, Davies JA, CGTP Collaborators. THE CONCISE GUIDE TO PHARMACOLOGY 2017/18: G protein-coupled receptors. British Journal of Pharmacology. 2017;174(Suppl 1):S17–S129.
28. Schiöth HB, Fredriksson R. The GRAFS classification system of G-protein coupled receptors in comparative perspective. General and comparative endocrinology. 2005; 142(1-2):94-101.
29. Gether U. "Uncovering molecular mechanisms involved in activation of G protein-coupled receptors." Endocrine Reviews. 2000;21(1):90-113.

30. Cabrera-Vera TM, Vanhauwe J, Thomas TO, Medkova M, Preininger A, Mazzoni MR, Hamm HE. Insights into G protein structure, function, and regulation. Endocrine Reviews. 2003;24(6):765–781.
31. Simon MI, Strathmann MP, Gautam N. Diversity of G proteins in signal transduction. Science, 1991; 252(5007):802-808.
32. Cordeaux Y, Hill SJ. "Mechanisms of cross-talk between G-protein-coupled receptors." Neurosignals. 2002;11(1):45–57.
33. Dahlgren C, Lind S, Mårtensson J, Björkman L, Wu Y, Sundqvist M, Forsman H. "G protein coupled pattern recognition receptors expressed in neutrophils: Recognition, activation/modulation, signaling and receptor regulated functions." Immunological Reviews. 2023;314(1):69–92.
34. Harden TK, Waldo GL, Hicks SN, Sondek J. "Mechanism of activation and inactivation of Gq/phospholipase C-β signaling nodes." Chemical Reviews. 2011;111(10):6120-6129.
35. Kozasa T, Jiang X, Hart MJ, Sternweis PM, Singer WD, Gilman AG, Bollag G, Sternweis PC. "p115 RhoGEF, a GTPase activating protein for Galpha12 and Galpha13." Science. 1998;280(5372):2109-2111.
36. Fromm C, Coso OA, Montaner S, Xu N, Gutkind JS. "The small GTP-binding protein Rho links G protein-coupled receptors and Galpha12 to the serum response element and to cellular transformation." Proceedings of the National Academy of Sciences USA. 1997;94(19):10098–10103.
37. Calebiro D, Koszegi Z, Lanoiselée Y, Miljus T, O'Brien S. G protein-coupled receptor-G protein interactions: a single-molecule perspective. Physiological Reviews. 2021;101(3):857–906.
38. Smrcka AV. G protein βγ subunits: central mediators of G protein-coupled receptor signaling. Cell Mol Life Sci, 2008; 65(14):2191-2214.
39. Lefkowitz RJ, Shenoy SK. "Transduction of receptor signals by beta-arrestins." Science. 2005;308(5721):512-517.
40. Lefkowitz RJ. "G protein-coupled receptors. III. New roles for receptor kinases and beta-arrestins in receptor signaling and desensitization." The Journal of Biological Chemistry. 1998;273(30):18677-18680.
41. Ferguson SS, Downey WE 3rd, Colapietro AM, Barak LS, Ménard L, Caron MG. "Role of beta-arrestin in mediating agonist-promoted G protein-coupled receptor internalization." Science. 1996;271(5247):363–366.
42. Wootten D, Christopoulos A, Marti-Solano M, Babu MM, Sexton PM. Mechanisms of signalling and biased agonism in G protein-coupled receptors. Nat Rev Mol Cell Biol, 2018; 19(10):638-653.
43. Goodman OB Jr, Krupnick JG, Santini F, Gurevich VV, Penn RB, Gagnon AW, Keen JH, Benovic JL. "Beta-arrestin acts as a clathrin adaptor in endocytosis of the beta2-adrenergic receptor." Nature. 1996;383(6599):447-450.
44. Gurevich VV, Gurevich EV. "GPCR Signaling Regulation: The Role of GRKs and Arrestins." Frontiers in Pharmacology. 2019;10:125.

45. Gainetdinov RR, Bohn LM, Sotnikova TD, Cyr M, Laakso A, Macrae AD, Torres GE, Kim KM, Lefkowitz RJ, Caron MG, Premont RT. "Dopaminergic supersensitivity in G protein-coupled receptor kinase 6-deficient mice." Neuron. 2003;38(2):291-303.
46. Lymperopoulos A, Rengo G, Funakoshi H, Eckhart AD, Koch WJ. "Adrenal GRK2 upregulation mediates sympathetic overdrive in heart failure." Nature Medicine. 2007;13(3):315-323.
47. Rajagopal S, Kim J, Ahn S, Craig S, Lam CM, Gerard NP, Gerard C, Lefkowitz RJ. Beta-arrestin- but not G protein-mediated signaling by the "decoy" receptor CXCR7. Proceedings of the National Academy of Sciences of the United States of America. 2010; 107(2):628-632.
48. Hilger D, Masureel M, Kobilka BK. "Structure and dynamics of GPCR signaling complexes." Nature Structural & Molecular Biology. 2018;25(1):4-12.
49. Venter JC, Adams MD, Myers EW, Li PW, Mural RJ, Sutton GG, Smith HO, Yandell M, Evans CA, Holt RA, Gocayne JD, Amanatides P, Ballew RM, Huson DH, Wortman JR, Zhang Q, Kodira CD, Zheng XH, Chen L, Skupski M, ... Zhu X. The sequence of the human genome. Science, 2001; 291(5507):1304-1351.
50. Lander ES, Linton LM, Birren B, Nusbaum C, Zody MC, Baldwin J, Devon K, Dewar K, Doyle M, FitzHugh W, Funke R, Gage D, Harris K, Heaford A, Howland J, Kann L, Lehoczky J, LeVine R, McEwan P, McKernan K, Meldrim J, Mesirov JP, ...Szustakowki J. "Initial sequencing and analysis of the human genome." Nature. 2001;409(6822):860-921.
51. International Human Genome Sequencing Consortium. "Finishing the euchromatic sequence of the human genome." Nature. 2004;431(7011):931–945.
52. Lagerström MC, Schiöth HB. "Structural diversity of G protein-coupled receptors and significance for drug discovery." Nature Reviews. Drug Discovery. 2008;7(4):339-357.
53. Tang XL, Wang Y, Li DL, Luo J, Liu MY. Orphan G protein-coupled receptors (GPCRs): biological functions and potential drug targets. Acta Pharmacol Sin, 2012; 33(3):363-371.
54. Crouch MF, Osmond RI. "New strategies in drug discovery for GPCRs: high throughput detection of cellular ERK phosphorylation." Combinatorial Chemistry & High Throughput Screening. 2008;11(5):344–356.
55. Bikkavilli RK, Tsang SY, Tang WM, Sun JX, Ngai SM, Lee SS, Ko WH, Wise H, Cheung WT. Identification and characterization of surrogate peptide ligand for orphan G protein-coupled receptor mas using phage-displayed peptide library. Biochemical Pharmacology. 2006;71(3):319–337.
56. Davenport AP, Alexander SP, Sharman JL, Pawson AJ, Benson HE, Monaghan AE, Liew WC, Mpamhanga CP, Bonner TI, Neubig RR, Pin JP, Spedding M, Harmar AJ. "International Union of Basic and Clinical Pharmacology. LXXXVIII. G protein-coupled receptor list: recommendations for new pairings with cognate ligands." Pharmacological Reviews. 2013;65(3):967–986.
57. Eggerickx D, Denef JF, Labbe O, Hayashi Y, Refetoff S, Vassart G, Parmentier M, Libert F. "Molecular cloning of an orphan G-protein-coupled receptor that constitutively activates adenylate cyclase." The Biochemical Journal. 1995;309(Pt 3):837–843.

58. Thathiah A, Spittaels K, Hoffmann M, Staes M, Cohen A, Horré K, Vanbrabant M, Coun F, Baekelandt V, Delacourte A, Fischer DF, Pollet D, De Strooper B, Merchiers P. The orphan G protein-coupled receptor 3 modulates amyloid-beta peptide generation in neurons. Science, 2009; 323(5916):946-951.
59. Zhang Y, Chen K, Sloan SA, Bennett ML, Scholze AR, O'Keeffe S, Phatnani HP, Guarnieri P, Caneda C, Ruderisch N, Deng S, Liddelow SA, Zhang C, Daneman R, Maniatis T, Barres BA, Wu JQ. An RNA-sequencing transcriptome and splicing database of glia, neurons, and vascular cells of the cerebral cortex. J Neurosci, 2014; 34(36):11929-11947.
60. Zeng Z, Su K, Kyaw H, Li Y. A novel endothelin receptor type-B-like gene enriched in the brain. Biochem Biophys Res Commun, 1997; 233(2):559-567.
61. Valdenaire O, Giller T, Breu V, Ardati A, Schweizer A, Richards JG. A new family of orphan G protein-coupled receptors predominantly expressed in the brain. FEBS Lett, 1998; 424(3):193-196.
62. Rezgaoui M, Süsens U, Ignatov A, Gelderblom M, Glassmeier G, Franke I, Urny J, Imai Y, Takahashi R, Schaller HC. The neuropeptide head activator is a high-affinity ligand for the orphan G-protein-coupled receptor GPR37. Journal of cell science. 2006; 119(Pt 3):542-549.
63. Bodenmüller H, Schaller HC. Conserved amino acid sequence of a neuropeptide, the head activator, from coelenterates to humans. Nature. 1981;293(5833):579–580.
64. Gandía J, Fernández-Dueñas V, Morató X, Caltabiano G, González-Muñiz R, Pardo L, Stagljar I, Ciruela F. "The Parkinson's disease-associated GPR37 receptor-mediated cytotoxicity is controlled by its intracellular cysteine-rich domain." Journal of Neurochemistry. 2013;125(3):362-372.
65. Dunham JH, Meyer RC, Garcia EL, Hall RA. "GPR37 surface expression enhancement via N-terminal truncation or protein-protein interactions." Biochemistry. 2009;48(43):10286–10297.
66. Southern C, Cook JM, Neetoo-Isseljee Z, Taylor DL, Kettleborough CA, Merritt A, Bassoni DL, et al. Screening β-arrestin recruitment for the identification of natural ligands for orphan G-protein-coupled receptors. J Biomol Screen, 2013; 18(5):599-609.
67. Smith NJ. Drug Discovery Opportunities at the Endothelin B Receptor-Related Orphan G Protein-Coupled Receptors, GPR37 and GPR37L1. Front Pharmacol, 2015; 6:275.
68. Kishimoto Y, Hiraiwa M, O'Brien JS. "Saposins: structure, function, distribution, and molecular genetics." Journal of Lipid Research. 1992;33(9):1255-1267.
69. Hineno T, Sano A, Kondoh K, Ueno S, Kakimoto Y, Yoshida K. "Secretion of sphingolipid hydrolase activator precursor, prosaposin." Biochemical and Biophysical Research Communications. 1991;176(2):668-674.
70. Meyer RC, Giddens MM, Coleman BM, Hall RA. The protective role of prosaposin and its receptors in the nervous system. Brain research. 2014; 1585:1-12.
71. Subramaniam S, Unsicker K. ERK and cell death: ERK1/2 in neuronal death. FEBS J, 2010; 277(1):22-29.
72. Campana WM, Hiraiwa M, O'Brien JS. "Prosaptide activates the MAPK pathway by a G-protein-dependent mechanism essential for enhanced sulfatide synthesis by Schwann cells." FASEB

Journal: Official Publication of the Federation of American Societies for Experimental Biology. 1998;12(3):307–314.

73. Ochiai T, Takenaka Y, Kuramoto Y, Kasuya M, Fukuda K, Kimura M, Shimeno H, Misasi R, Hiraiwa M, Soeda S. Molecular mechanism for neuro-protective effect of prosaposin against oxidative stress: its regulation of dimeric transcription factor formation. Biochimica et biophysica acta. 2008; 1780(12):1441-1447.
74. Brunet A, Datta SR, Greenberg ME. Transcription-dependent and -independent control of neuronal survival by the PI3K-Akt signaling pathway. Current Opinion in Neurobiology. 2001;11(3):297–305.
75. Alexander SP, Benson HE, Faccenda E, Pawson AJ, Sharman JL, Spedding M, Peters JA, Harmar AJ, CGTP Collaborators. The Concise Guide to PHARMACOLOGY 2013/14: G protein-coupled receptors. British Journal of Pharmacology. 2013;170(8):1459–1581.
76. Lundius EG, Vukojevic V, Hertz E, Stroth N, Cederlund A, Hiraiwa M, Terenius L, Svenningsson P. "GPR37 protein trafficking to the plasma membrane regulated by prosaposin and GM1 gangliosides promotes cell viability." The Journal of Biological Chemistry. 2014;289(8):4660-4673.
77. Liu B, Mosienko V, Vaccari Cardoso B, Prokudina D, Huentelman M, Teschemacher AG, Kasparov S. "Glio- and neuro-protection by prosaposin is mediated by orphan G-protein coupled receptors GPR37L1 and GPR37." Glia. 2018;66(11):2414-2426.
78. Bang S, Xie YK, Zhang ZJ, Wang Z, Xu ZZ, Ji RR. GPR37 regulates macrophage phagocytosis and resolution of inflammatory pain. Journal of Clinical Investigation. 2018;128(8):3568–3582.
79. Qian Z, Li H, Yang H, Yang Q, Lu Z, Wang L, Chen Y, Li X. Osteocalcin attenuates oligodendrocyte differentiation and myelination via GPR37 signaling in the mouse brain. Science advances. 2021; 7(43):eabi5811.
80. Bang S, Donnelly CR, Luo X, Toro-Moreno M, Tao X, Wang Z, Chandra S, Bortsov AV, Derbyshire ER, Ji RR. Activation of GPR37 in macrophages confers protection against infection-induced sepsis and pain-like behaviour in mice. Nature Communications. 2021;12(1):1704.
81. Qian Z, Liu C, Li H, Yang H, Wu J, Liu J, Li Y, Chen X, Xu J, Li X. Osteocalcin alleviates lipopolysaccharide-induced acute inflammation via activation of GPR37 in macrophages. Biomedicines. 2022; 10(5):1006.
82. Alexander SPH, Christopoulos A, Davenport AP, Kelly E, Mathie A, Peters JA, Veale EL, Armstrong JF, Faccenda E, Harding SD, Pawson AJ, Sharman JL, Southan C, Davies JA, CGTP Collaborators. THE CONCISE GUIDE TO PHARMACOLOGY 2019/20: G protein-coupled receptors. British Journal of Pharmacology. 2019;176(Suppl 1):S21–S141.
83. Morató X, Garcia-Esparcia P, Argerich J, Llorens F, Zerr I, Paslawski W, Borràs E, Sabidó E, Petäjä-Repo UE, Fernández-Dueñas V, Ferrer I, Svenningsson P, Ciruela F. Ecto-GPR37: a potential biomarker for Parkinson's disease. Translational neurodegeneration. 2021; 10(1):8.

84. Murakami T, Shoji M, Imai Y, Inoue H, Kawarabayashi T, Matsubara E, Harigaya Y, Sasaki A, Takahashi R, Abe K. Pael-R is accumulated in Lewy bodies of Parkinson's disease. Annals of neurology. 2004; 55(3):439-442.
85. Marazziti D, Di Pietro C, Golini E, Mandillo S, Matteoni R, Tocchini-Valentini GP. Macroautophagy of the GPR37 orphan receptor and Parkinson disease-associated neurodegeneration. Autophagy. 2009; 5(5):741-742.
86. Imai Y, Soda M, Takahashi R. "Parkin suppresses unfolded protein stress-induced cell death through its E3 ubiquitin-protein ligase activity." The Journal of Biological Chemistry. 2000;275(46):35661-35664.
87. Lundius EG, Stroth N, Vukojević V, Terenius L, Svenningsson P. "Functional GPR37 trafficking protects against toxicity induced by 6-OHDA, MPP+ or rotenone in a catecholaminergic cell line." Journal of Neurochemistry. 2013;124(3):410-417.
88. Kubota K, Niinuma Y, Kaneko M, Okuma Y, Sugai M, Omura T, Uesugi M, Uehara T, Hosoi T, Nomura Y. "Suppressive effects of 4-phenylbutyrate on the aggregation of Pael receptors and endoplasmic reticulum stress." Journal of Neurochemistry. 2006;97(5):1259-1268.
89. Cantley LC. "The phosphoinositide 3-kinase pathway." Science. 2002;296(5573):1655–1657.
90. Martelli AM, Evangelisti C, Chiarini F, McCubrey JA. The phosphatidylinositol 3-kinase/Akt/mTOR signaling network as a therapeutic target in acute myelogenous leukemia patients. Oncotarget. 2010; 1(2):89-103.
91. Law NC, White MF, Hunzicker-Dunn ME. "G protein-coupled receptors (GPCRs) That Signal via Protein Kinase A (PKA) Crosstalk at Insulin Receptor Substrate 1 (IRS1) to Activate the phosphatidylinositol 3-kinase (PI3K)/AKT Pathway." The Journal of Biological Chemistry. 2016;291(53):27160-27169.
92. New DC, Wu K, Kwok AW, Wong YH. G protein-coupled receptor-induced Akt activity in cellular proliferation and apoptosis. The FEBS journal. 2007; 274(23):6025-6036.
93. Manning BD, Cantley LC. AKT/PKB signaling: navigating downstream. Cell. 2007; 129(7):1261-1274.
94. Roy T, Boateng ST, Uddin MB, Banang-Mbeumi S, Yadav RK, Bock CR, Folahan JT, Siwe-Noundou X, Walker AL, King JA, Buerger C, Huang S, Chamcheu JC. The PI3K-Akt-mTOR and associated signaling pathways as molecular drivers of immune-mediated inflammatory skin diseases: update on therapeutic strategy using natural and synthetic compounds. Cells. 2023; 12(12):1671.
95. Glaviano A, Foo ASC, Lam HY, et al. "PI3K/AKT/mTOR signaling transduction pathway and targeted therapies in cancer." Molecular Cancer. 2023;22(1):138.
96. Santini E, Heiman M, Greengard P, Valjent E, Fisone G. Inhibition of mTOR signaling in Parkinson's disease prevents L-DOPA-induced dyskinesia. Science signaling. 2009; 2(80):ra36.
97. Desale SE, Chidambaram H, Chinnathambi S. "G-protein coupled receptor, PI3K and Rho signaling pathways regulate the cascades of Tau and amyloid-β in Alzheimer's disease." Molecular Biomedicine. 2021;2(1):17.

98. Nechamen CA, Thomas RM, Cohen BD, Acevedo G, Poulikakos PI, Testa JR, Dias JA. Human follicle-stimulating hormone (FSH) receptor interacts with the adaptor protein APPL1 in HEK 293 cells: potential involvement of the PI3K pathway in FSH signaling. Biology of reproduction. 2004; 71(2):629-636.
99. Suh JM, Song JH, Kim DW, Kim H, Chung HK, Hwang JH, Kim JM, Hwang ES, Chung J, Han JH, Cho BY, Ro HK, Shong M. Regulation of the phosphatidylinositol 3-kinase, Akt/protein kinase B, FRAP/mammalian target of rapamycin, and ribosomal S6 kinase 1 signaling pathways by thyroid-stimulating hormone (TSH) and stimulating type TSH receptor antibodies in the thyroid gland. J Biol Chem, 2003; 278(24):21960-21971.
100. Ye X, Ishii I, Kingsbury MA, Chun J. Lysophosphatidic acid as a novel cell survival/apoptotic factor. Biochim Biophys Acta, 2002; 1585(2-3):108-113.
101. Zamani A, Qu Z. Serotonin activates angiogenic phosphorylation signaling in human endothelial cells. FEBS Lett, 2012; 586(16):2360-2365.
102. Kim EK, Yun SJ, Do KH, Kim MS, Cho M, Suh DS, Kim CD, Kim JH, Birnbaum MJ, Bae SS. "Lysophosphatidic acid induces cell migration through the selective activation of Akt1." Experimental & Molecular Medicine. 2008;40(4):445-452.
103. Liu F, Zhu C, Huang X, Cai J, Wang H, Wang X, He S, Liu C, Yang X, Zhang Y, Zhang T. "A low level of GPR37 is associated with human hepatocellular carcinoma progression and poor patient survival." Pathology, Research and Practice. 2014;210(12):885-892ub
104. Zhang Y, Wang L. Up-regulation of GPR37 promotes the proliferation of human glioma U251 cells. Xi Bao Yu Fen Zi Mian Yi Xue Za Zhi, 2018; 34(4):341-345.
105. Zhang J, Xie L, Li H, Li S, Gao X, Zhang M. Selenomethionine Promotes Milk Protein and Fat Synthesis and Proliferation of Mammary Epithelial Cells through the GPR37-mTOR-S6K1 Signaling. J Agric Food Chem, 2024; 72(35):19505-19516.
106. Yu J, Li J, Matei N, Wang W, Tang L, Pang J, Li X, Fang L, Tang J, Zhang JH, Yan M. Intranasal administration of recombinant prosaposin attenuates neuronal apoptosis through GPR37/PI3K/Akt/ASK1 pathway in MCAO rats. Exp Neurol, 2024; 373:114656.
107. Scott RE. Plasma membrane vesiculation: a new technique for isolation of plasma membranes. Science. 1976; 194(4266):743-745.
108. Levental KR, Levental I. "Giant plasma membrane vesicles: models for understanding membrane organization." Current Topics in Membranes. 2015;75:25-57.
109. Sezgin E. Giant plasma membrane vesicles to study plasma membrane structure and dynamics. Biochimica et biophysica acta. Biomembranes. 2022; 1864(4):183857.
110. Worch R, Petrášek Z, Schwille P, Weidemann T. Diffusion of Single-Pass Transmembrane Receptors: From the Plasma Membrane into Giant Liposomes. J Membr Biol, 2017; 250(4):393-406.
111. Diekmann S, Hoischen C. "Biomolecular dynamics and binding studies in the living cell." Physics of Life Reviews. 2014;11(1):1–30.

112. Yu L, Lei Y, Ma Y, Liu M, Zheng J, Dan D, Gao P. A Comprehensive Review of Fluorescence Correlation Spectroscopy. Front Phys, 2021; 9:644450.
113. Kilpatrick LE, Hill SJ. "The use of fluorescence correlation spectroscopy to characterize the molecular mobility of fluorescently labelled G protein-coupled receptors." Biochemical Society Transactions. 2016;44(2):624-629.
114. Briddon SJ, Kilpatrick LE, Hill SJ. Studying GPCR Pharmacology in Membrane Microdomains: Fluorescence Correlation Spectroscopy Comes of Age. Trends in Pharmacological Sciences. 2018;39(2):158–174.
115. Waithe D. Open-source browser-based software simplifies fluorescence correlation spectroscopy data analysis. Nat Photonics, 2021; 15:790-791.
116. Sonawane ND, Szoka FC Jr, Verkman AS. Chloride accumulation and swelling in endosomes enhances DNA transfer by polyamine-DNA polyplexes. J Biol Chem, 2003; 278(45):44826-44831.

8 CURRICULUM VITAE